AMERICAN SOCIETY FOR MICROBIOLOGY | Journal of Virology®

PATHOGENESIS AND IMMUNITY

Time Series Transcriptomic Analysis of Bronchoalveolar Lavage Cells from Piglets Infected with Virulent or Low-Virulent Porcine Reproductive and Respiratory Syndrome Virus 1

J. M. Sánchez-Carvajal,[a] I. M. Rodríguez-Gómez,[a] I. Ruedas-Torres,[a] S. Zaldívar-López,[b] F. Larenas-Muñoz,[a] R. Bautista-Moreno,[c] J. J. Garrido,[b] F. J. Pallarés,[a] L. Carrasco,[a] J. Gómez-Laguna[a]

[a]Department of Anatomy and Comparative Pathology and Toxicology, Faculty of Veterinary Medicine, University of Córdoba, Córdoba, Spain
[b]Department of Genetics, Faculty of Veterinary Medicine, University of Córdoba, Córdoba, Spain
[c]Andalusian Platform of Bioinformatic, University of Málaga, Campanillas, Málaga, Spain

ABSTRACT Porcine reproductive and respiratory syndrome virus (PRRSV) has evolved to escape the immune surveillance for a survival advantage leading to a strong modulation of host's immune responses and favoring secondary bacterial infections. However, limited data are available on how the immunological and transcriptional responses elicited by virulent and low-virulent PRRSV-1 strains are comparable and how they are conserved during the infection. To explore the kinetic transcriptional signature associated with the modulation of host immune response at lung level, a time-series transcriptomic analysis was performed in bronchoalveolar lavage cells upon experimental *in vivo* infection with two PRRSV-1 strains of different virulence, virulent subtype 3 Lena strain or the low-virulent subtype 1 3249 strain. The time-series analysis revealed overlapping patterns of dysregulated genes enriched in T-cell signaling pathways among both virulent and low-virulent strains, highlighting an upregulation of co-stimulatory and co-inhibitory immune checkpoints that were disclosed as Hub genes. On the other hand, virulent Lena infection induced an early and more marked "negative regulation of immune system process" with an overexpression of co-inhibitory receptors genes related to T-cell and NK cell functions, in association with more severe lung lesion, lung viral load, and BAL cell kinetics. These results underline a complex network of molecular mechanisms governing PRRSV-1 immunopathogenesis at lung level, revealing a pivotal role of co-inhibitory and co-stimulatory immune checkpoints in the pulmonary disease, which may have an impact on T-cell activation and related pathways. These immune checkpoints, together with the regulation of cytokine-signaling pathways, modulated in a virulence-dependent fashion, orchestrate an interplay among pro- and anti-inflammatory responses.

IMPORTANCE Porcine reproductive and respiratory syndrome virus (PRRSV) is one of the major threats to swine health and global production, causing substantial economic losses. We explore the mechanisms involved in the modulation of host immune response at lung level performing a time-series transcriptomic analysis upon experimental infection with two PRRSV-1 strains of different virulence. A complex network of molecular mechanisms was revealed to control the immunopathogenesis of PRRSV-1 infection, highlighting an interplay among pro- and anti-inflammatory responses as a potential mechanism to restrict inflammation-induced lung injury. Moreover, a pivotal role of co-inhibitory and co-stimulatory immune checkpoints was evidenced, which may lead to progressive dysfunction of T cells, impairing viral clearance and leading to persistent infection, favoring as well secondary bacterial infections or viral rebound. However, further studies should be conducted to evaluate the functional role of immune checkpoints in advanced stages of PRRSV infection and explore a possible T-cell exhaustion state.

Editor Tom Gallagher, Loyola University Chicago

Address correspondence to J. M. Sánchez-Carvajal, v42sancj@uco.es.

The authors declare no conflict of interest.

Received 7 July 2021
Accepted 15 November 2021
Accepted manuscript posted online 1 December 2021
Published 9 February 2022

KEYWORDS porcine reproductive and respiratory syndrome virus, virulence, bronchoalveolar lavage cells, time-series transcriptomic analysis, Hub genes, immune checkpoints, T-cells

Porcine reproductive and respiratory syndrome virus (PRRSV) is the major hazard to swine health and global production, causing dramatic economic losses (1, 2) due to reproductive failure in pregnant sows and respiratory disorders in growing pigs (3, 4). PRRSV encompasses two species, *Betaarterivirus suid 1* and *Betaarterivirus suid 2* (PRRSV-1 and PRRSV-2, respectively) (5), which present a wide inter- and intra-species viral and antigenic diversity (6–8). PRRSV shows signs of a marked mutation rate, favoring the emergence and re-emergence of virulent strains worldwide, which has gained special interest since 2006. PRRSV-1 virulent strains have been reported to induce high morbidity and mortality rates, fever, hemorrhages, severe lung damage, and, eventually, lesions in other organs (9–11, 13–15), increasing the concern for understanding the immunopathology of PRRSV.

PRRSV has evolved a variety of strategies to manipulate, even to evade, the host antiviral innate immunity and some cellular survival-associated pathways, facilitating its replication and distribution (16, 17). An impairment of type I interferon (IFN-I) signaling cascade and production, modulation of cytokine expression by immune cells as well as antigen presentation and T-cell activation, has been described for PRRSV infection (16, 18–22). Indeed, this dysregulation of host's immune responses (18, 20) is bound to persistent infection and to facilitation of secondary bacterial infections, resulting in porcine respiratory disease complex (PRDC) (23).

High-throughput RNA sequencing (RNA-seq) technology combined with bioinformatic analysis has emerged as an essential tool to acquire relevant knowledge about cellular signaling pathways (24). Thereby, transcriptome analysis of bronchoalveolar lavage (BAL) cells, which reflects immune and pathological changes in the lung, would be an accurate approach to reveal dynamic changes in the host cellular responses against viral infection, shedding new light on PRRSV-1 immunopathogenesis at lung level.

Previous studies have explored changes in RNA-seq profile upon PRRSV infection using only one strain, mainly PRRSV-2, and determining these changes by means of microarrays, which have weaknesses relying on existing knowledge about the genome sequence (25, 26). Unlike *in vivo* studies, *in vitro* approaches present serious difficulties in identifying how the host response interacts with PRRSV, given the impossibility of connecting different cell subpopulations and cellular microenvironments (27–30). Relatively few studies have evaluated RNA-seq changes at tissue level (24), and besides, most of them conducted the analysis at 1 or 2 time points in a single tissue after PRRSV infection, frequently lymphoid tissues, which are not the main target organ for PRRSV (31, 32).

Therefore, the present study aims to explore the mechanisms involved in the modulation of host immune response at lung level, performing a time-series analysis upon experimental infection with two PRRSV-1 strains of different virulence, low-virulent 3249 strain and virulent Lena strain, identifying those terms that are conserved or strain specific in the early stages of the infection.

RESULTS

Lena-infected piglets exhibited hyperthermia and marked clinical signs associated with severe interstitial pneumonia, acute suppurative bronchopneumonia, and the highest lung viral load. Gross lesions and histopathology were thoroughly described by Rodríguez-Gómez et al. (40). In brief, PRRSV-1-infected piglets exhibited clinical signs associated with respiratory disease. Furthermore, virulent Lena-infected pigs presented hyperthermia for a long period (mean above 40.5°C) with marked clinical signs, which reached the maximum at 6 dpi. At necropsy, lung macroscopic lesion score increased gradually throughout the study in both PRRSV-1-infected groups, due to

severe interstitial pneumonia and getting to the highest score in the Lena group for the additional presence of extensive areas of pulmonary consolidation in cranial and middle lobes from 6 dpi onwards, which was confirmed by histopathological evaluation. Virulent Lena strain induced an earlier (2 out of 5 piglets PRRSV-1 positive at 1 dpi) and higher replication in the lung compared to low-virulent 3249 strain ($P < 0.01$ at 3 dpi; $P < 0.05$ at 6 and 8 dpi), displaying a lung viral load peak at 6 (Cq 18.9 $\pm$ 0.9) and 8 dpi (Cq 22.9 $\pm$ 2.5), respectively (Fig. 1A). Control animals did not show clinical signs and minimal lung lesion, remaining as RT-qPCR-negative for PRRSV-1 throughout the study.

CD163$^+$ cells decreased within live PAMs together with a mixed influx of neutrophils, monocytes, and lymphocytes in BAL cells of Lena-infected pigs. FCM analysis in BAL cells were thoroughly described by Rodríguez-Gómez et al. (2019). Briefly, CD163 expression was studied only in live BAL cells from either control or PRRSV-infected pigs. Control animals showed a homogeneous and stable subset of cells within live PAMs, compatible with PAMs because of size and granularity properties as well as CD163 labeling, throughout the study (Fig. 1B, red circle, and Fig. 1C). By contrast, both subsets, PAMs and CD163$^+$ cells, decreased alongside the study in PRRSV-1-infected pigs (Fig. 1B, red arrows, and 1C). This drop was more marked and occurred earlier (3 dpi) in Lena-infected pigs than in 3249 group (8 dpi) and was accompanied by a mixture of neutrophils, monocytes, and, to a lesser extent, lymphocytes (Fig. 1B, green circle) from 6 dpi onwards in Lena-infected pigs and at 13 dpi in 3249-infected animals.

Time-series differential gene expression pattern related to PRRSV-1 infection. A total of 1,935 and 8,352 significant variable genes were detected by MasigPro during the time course for 3249- and Lena-infected pigs, respectively. After clustering, these significant variable genes were subdivided into 5 different clusters according to their expression profiles, thus, the genes included within a cluster presented a similar expression pattern. Fig. 2 illustrates the median expression level of clusters 3, 4, and 5 at each time point. Clusters 1 and 2 showed an inconsistent trend among experimental groups. Cluster 3 consisted of 98 genes whose median expression level increased in 3249-infected piglets from 8 dpi throughout the study, but this increase was higher and earlier, from 6 dpi, in Lena-infected piglets. GO enrichment-functional analyses were performed to gain biological understanding of variable genes included in cluster 3, which were mainly enriched in GO involved in "regulation of immune system process," "leukocyte differentiation," "regulation of cytokine production," "negative regulation of immune system process," "lymphocyte activation," "response to cytokine," and "positive regulation of apoptotic process" (Fig. 2A). Genes in cluster 4, a total of 59, followed a similar kinetics to the one described above for cluster 3 in 3249-infected piglets, but for Lena-infected pigs, the expression of these genes had a marked and rapid increase from 1 to 3 dpi remaining roughly constant throughout the study (Fig. 2). The significantly enriched GO terms related to cluster 4 were "cytokine-mediated signaling pathway," "response to bacterium," "regulation of cytokine production," "IFN-I signaling pathway," and "cellular response to tumor necrosis factor" (genes and pathways are listed in Fig. 2B). Cluster 5 comprised 45 genes whose expression rose from 8 to 13 dpi in both infected groups (Fig. 2). Genes in cluster 5 were involved in the GO terms "lipid transport" and "carboxylic acid transport" (Fig. 2C).

DEGs profile in BAL cells of PRRSV-1-infected piglets. DEGs were identified in response to 3249 or Lena infection by comparing the gene expression levels of PRRSV-1-infected animals to control animals at each time point using an $FDR < 0.05$ and a log2FC $\geq$ 1.0 (upregulated genes) or log2FC $\leq$ –1.0 (downregulated genes) as the cutoff criteria. Thus, a total of 14,368 DEGs in 3249 data set and 11,656 DEGs in Lena data set were found to be differentially expressed along the study (Fig. 3A and B).

Similar dynamic changes in the gene expression level were observed in both 3249- and Lena-infected piglets, with an increasing number of DEGs along the study. As expected, in both infected groups, the lowest number of DEGs was observed at 1 dpi (data not showed). At 3 dpi, 38 DEGs (downregulated: 5; upregulated: 33) and 863

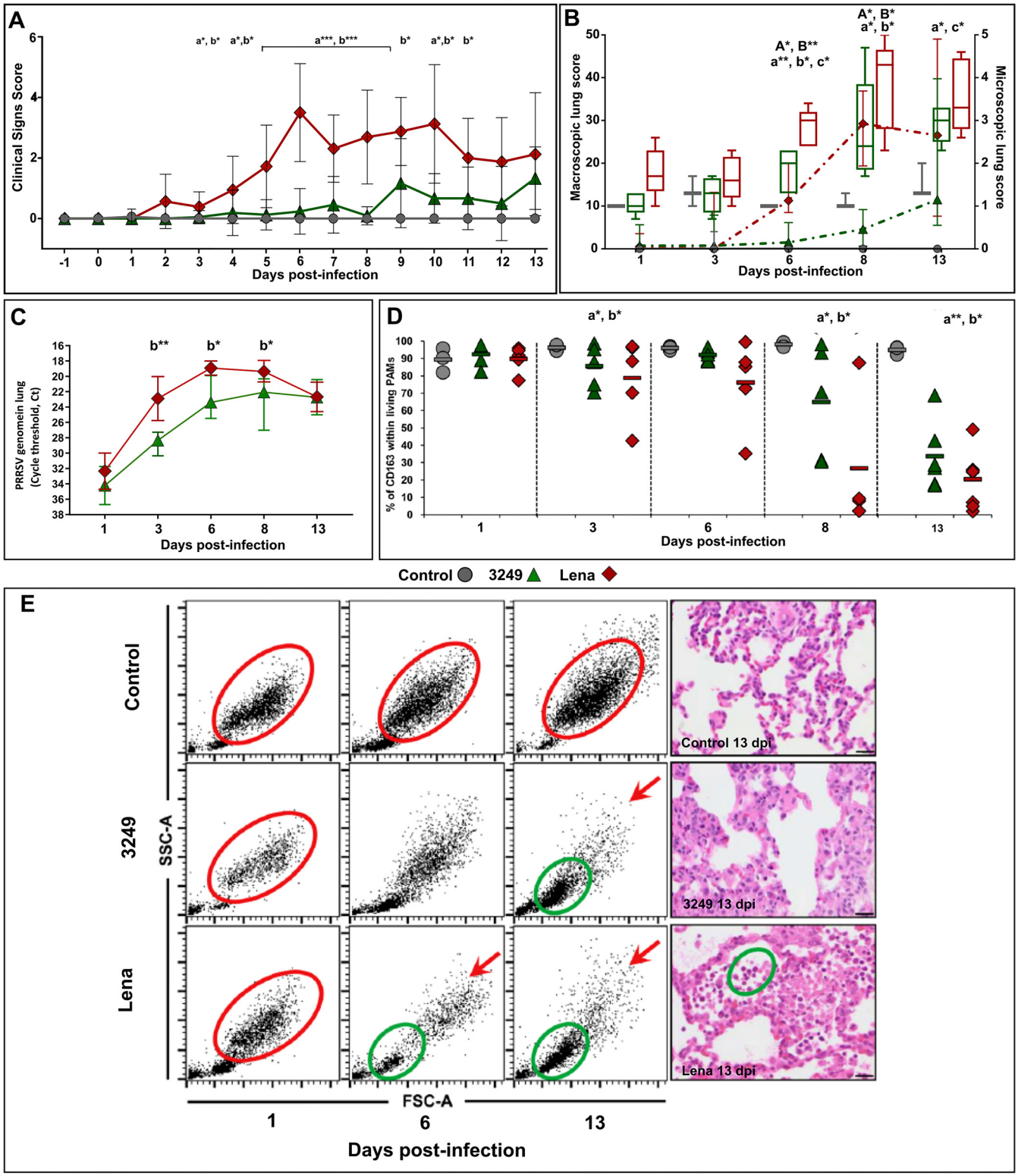

FIG 1 PRRSV lung viral load was quantified by RT-qPCR (A). Viral load is represented by changes in the quantification cycle (Cq) (control, gray circles; 3249, green triangles; Lena, red diamonds). Frequency of live CD163$^+$ PAMs (B). Freshly isolated BAL cells from control and PRRSV-1-infected pigs were stained and analyzed for the expression of CD163 by FCM. The scatter dot plot shows the frequency of CD163$^+$ cells in control, 3249, and Lena group along the experimental infection. Changes in BAL cells subpopulation by FCM (FSC-A versus SSC-A) according to histopathological findings from a representative pig of the control, 3249, and Lena infected group at 1, 6, and 13 dpi (C). Red circles indicate living potential PAMs according to light scatter properties (size and granularity). Red arrows show the decrease of the above-mentioned subset in 3249- and Lena-infected pigs. Green circles indicate a mixture of neutrophils, monocytes, and, to a lesser extent, lymphocytes, according to light scatter properties. Microscopic pictures for each representative animal at 13 dpi supporting FCM findings. Bars, 20 μm. Statistical differences between groups are indicated (*, $P < 0.05$; **, $P < 0.01$).

A

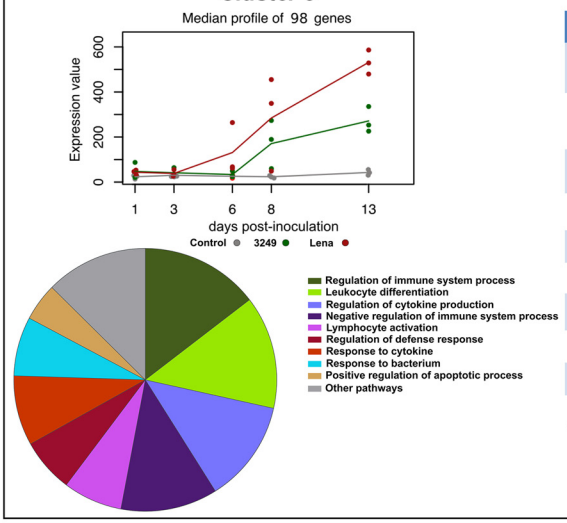

GO Term		% Associated Genes / Term	Number of genes	Associated Genes Found
Regulation of immune system process		1.26	22.00	ADIPOQ, CD3D, CD8A, CD96, CLDN18, CTLA4, CX3CR1, DDX60, DLG5, ETS1, GBP1, IKZF3, ITK, PARP9, PDE4D, PRKCA, PTPN22, RORA, SAMHD1, SH2D1A, THEMIS, TIGIT
Leukocyte differentiation		2.14	21.00	ADIPOQ, ANKRD1, CCR4, CD3D, CD8A, CD96, CLDN18, GBP1, ETS1, CTLA4, DLG5, IKZF3, ITK, PRKCA, PTPN22, RORA, SNRK, SATB1, SAMHD1, THEMIS, TIGHT
Regulation of cytokine production		1.41	19.00	ADIPOQ, CD96, CTLA4, CX3CR1, DDX60, DCLK2, DUSP4, GBP1, HEG1, ITGA1, MAK4, PRKCA, PDE4D, PTPN22, RNF128, RORA, SH2D1A, SNRK, TIGIT
Negative regulation of immune system process		2.11	18.00	ADIPOQ, ATP1B2, CD96, CLDN18, CTLA4, CX3CR1, DLG5, ETS1, IKZF3, LAMA3, GBP1, PCDH18, PRKCA, PTPN22, RNF128, SAMHD1, SH2D1A, TIGIT
Lymphocyte activation		1.33	11.00	CD3D, CD8A, CTLA4, DLG5, IKZF3, ITK, PTPN22, RORA, SATB1, THEMIS, TIGIT
Regulation of defense response		1.37	10.00	ADIPOQ, CD96, DDX60, ETS1, PARP9, PRKCA, PTPN22, RORA, SAMHD1, SH2D1A
Response to cytokine		1.02	13.00	ADIPOQ, ANKRD1, CCR4, CLDN18, CX3CR1, ETS1, GBP1, GBP7, PARP9, PRKCA, RORA, SAMHD1, TNFRSF9
Response to bacterium		1.36	11.00	ADIPOQ, ANKRD1, CCR4, CD96, CX3CR1, GBP7, GZMA, IKZF3, PDE4D, PRKCA, PTPN22
Positive regulation of apoptotic process		1.02	7.00	ADIPOQ, ANKRD1, ARHGEF3, CTLA4, GZMA, ITGA1, MCF2L
Circulatory system process		1.33	9.00	ABCB1, ADIPOQ, ATP1B2, F5, HEG1, ITGA1, PDE4D, PRKCA, SLC44A1
Regulation of cytosolic calcium ion concentration	*Other pathways*	1.34	5.00	CCR4, CX3CR1, P2RY10, PDE4D, PRKCA
Peptidyl-tyrosine phosphorylation		1.21	5.00	ADIPOQ, ITK, PARP9, PTPN22, RORA

B

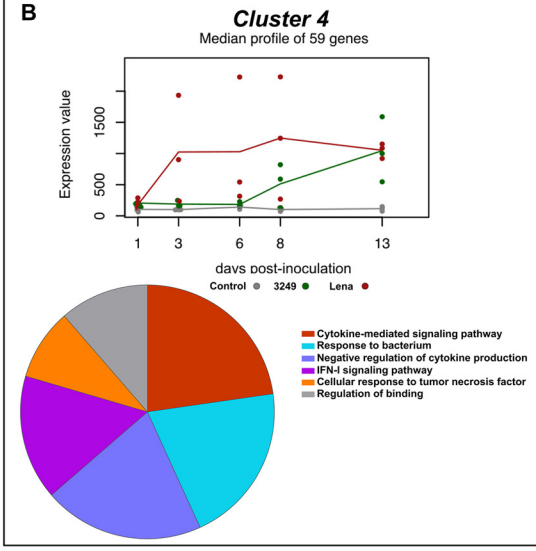

GO Term	% Associated Genes / Term	Number of genes	Associated Genes Found
Cytokine-mediated signaling pathway	1.19	10.00	CCL20, CSF3, EDN1, IFIT1, IFIT2, IL1R2, ISG15, RSAD2, TNFAIP3, TNFRSF4
Response to bacterium	1.11	9.00	C15orf48, CCL20, CMPK2, CSF3, EDN1, ISG15, PDE4B, PLAC8, TNFAIP3
Regulation of cytokine production	1.15	9.00	HERC5, IL1R2, ISG15, MMP8, PDE4B, RSAD2, SORL1, TNFAIP3, TNFRSF4
IFN-I signaling pathway	4.17	7.00	HERC5, IFI44L, IFIT1, IFIT2, ISG15, RSAD2, TNFAIP3
Cellular response to tumor necrosis factor	1.32	4.00	CCL20, EDN1, TNFAIP3, TNFRSF4
Regulation of binding	1.29	5.00	CSF3, IFIT1, IFIT2, MMP8, SORL1

C

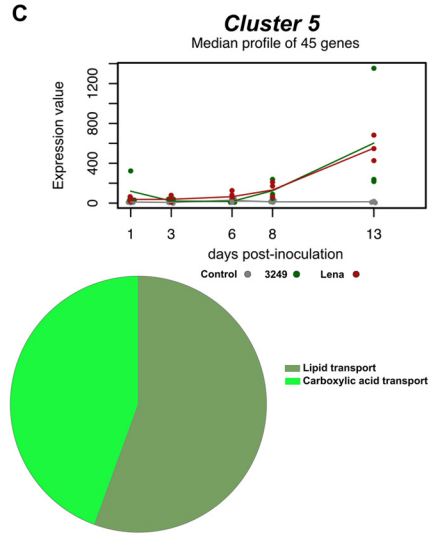

GO Term	% Associated Genes / Term	Number of genes	Associated Genes Found
Lipid transport	1.20	5.00	ACE, AQP9, CD36, LIPG, SPP1
Carboxylic acid transport	1.45	4.00	ACE, AQP9, CD36, SLC47A1

FIG 2 MaSigPro analysis of RNA-seq time-series data set. Clusters 3 (A), 4 (B), and 5 (C) showed distinct temporal profiles associated with low-virulent 3249 and virulent Lena strain infection. The median expression of all genes in each cluster was plotted for control (gray), 3249 (green),

(Continued on next page)

DEGs (downregulated: 110; upregulated: 753) were found in 3249- and Lena-infected piglets, respectively; and at 6 dpi, 5,860 DEGs (downregulated: 1,193; upregulated: 4,667) and 4,190 DEGs (downregulated: 1,195; upregulated: 2,995) were identified. At 8 dpi, a lower number of DEGs was observed probably due to cell death phenomena, with 1,155 DEGs (downregulated: 46; upregulated: 1,109) for 3249 and 2,003 DEGs (downregulated: 85; upregulated: 1918) for Lena. The highest number of DEGs were found at 13 dpi with 7,315 genes (downregulated: 3,886; upregulated: 3,429) and 4,600 genes (downregulated: 1,556; upregulated: 3,044) differentially expressed for 3249 and Lena groups, respectively (Fig. 3A and B).

Identification and functional classification of conserved DEGs in response to 3249 strain infection. A total of 14,368 DEGs were identified in response to 3249 infection during the study. Most of the DEGs (9,218) were expressed at only one of the evaluated time points, hence, we focused on those DEGs that were conserved in two or more time points, to achieve a better understanding of the infection. Thus, whereas no DEGs were concomitantly identified during the early time points of infection (1 or 3 dpi), 96 overlapped DEGs were found at 6–8–13 dpi, of which 13 genes were downregulated and 83 were upregulated (Fig. 4A). To gain further insight into the potential functions of these 96 DEGs, a functional-enrichment analysis based on the GO database was performed to explore BPs and ISPs. The significantly enriched GO terms with a $P\ value < 0.05$ are illustrated in Fig. 4B to D. The results of the GO analysis reported that most DEGs were mainly involved in the "innate immune response" (17 DEGs, 28.80%), "MAPK cascade" (11 DEGs, 18.64%), "defense response to virus" (6 DEGs, 7.55%), "regulation of JNK cascade" (5 DEGs, 8.47%), "cellular response to interferon γ (IFN-γ)" (5 DEGs, 8.47%), and "regulation of α/β T-cell activation" (4 DEGs, 6.78%), among others. The patterns of expression of representative genes for low-virulent 3249 strain are illustrated in Fig. 4C. Fig. 4B-4D list the symbol and number of genes enriched in each GO term.

Moreover, the number of conserved DEGs increased at 8–13 dpi, with 854 DEGs identified at these time points (Fig. 4A). Among these genes, only 16 genes were downregulated, whereas 838 were upregulated. In this case, the GO functional-enrichment analysis (BPs and ISPs categories) revealed that T-cell-related pathways were significantly altered with 7 different GO terms ("T-cell co-stimulation," "regulation of α/β T-cell differentiation," "T-cell selection," "regulation of T-cell receptor signaling pathway," "regulatory T-cell differentiation," "$CD8^+$ α/β T-cell activation," and "$CD4^+CD25^+$ α/β T-cell differentiation") and an occurrence of enriched genes over 50%. In addition, other highly enriched GO terms were related to "regulation of interleukin-2 (IL-2) production" (17 DEGs, 14.41%), "regulation of lymphocyte chemotaxis" (9 DEGs, 7.63%), or "regulation of tolerance induction" (6 DEGs, 5.08%). Fig. 5A and B list the symbol and number of genes enriched in each GO term.

PPI network construction and Hub genes identification for 3249 infection. The PPI network was constructed with the 854 conserved DEGs found at 8 and 13 dpi by the STRING database, with 402 nodes and 2,400 edges. The Hub genes were selected from the whole PPI network using the MCC and DMNC algorithm of the CytoHubba plugin. According to the MCC and DMNC scores, the top 10 highest-scored genes found for each approach include *PDCD1*, *LAG3*, *TNFRSF18*, *ICOS*, *CD8A*, *CD6*, *CTLA4*, *CD28*, *GZMB*, *TBX21*, *SELL*, *IL7R*, *IL2RA*, *IL2RB*, *PRF1*, *FASLG*, *KLRK1*, *CD226* and *CD40LG* (Fig. 6A and B). Also, the kinetic of expression of these genes is illustrated in Fig. 6C–6D. Because of the complexity, the whole PPI network was analyzed using the MCODE plugin to identify essential PPI network modules, making the understanding of molecular mechanisms more approachable. The top 3 significant clusters with a k-core > 6 were named as A, B,

FIG 2 Legend (Continued)
and Lena strain (red) along the different time points. Solid lines depicting the median and solid plots show the individual value. Gene Ontology (GO) analysis of clusters 3 (A), 4 (B), and 5 (C). ClueGO and CluePedia were used to conduct a functional enrichment analysis. Tables list the top terms of GO biological processes (BPs) and immune system processes (ISPs) associated with genes grouped in each cluster over time. Overview pie chart shows the proportion of genes associated with the top functional groups.

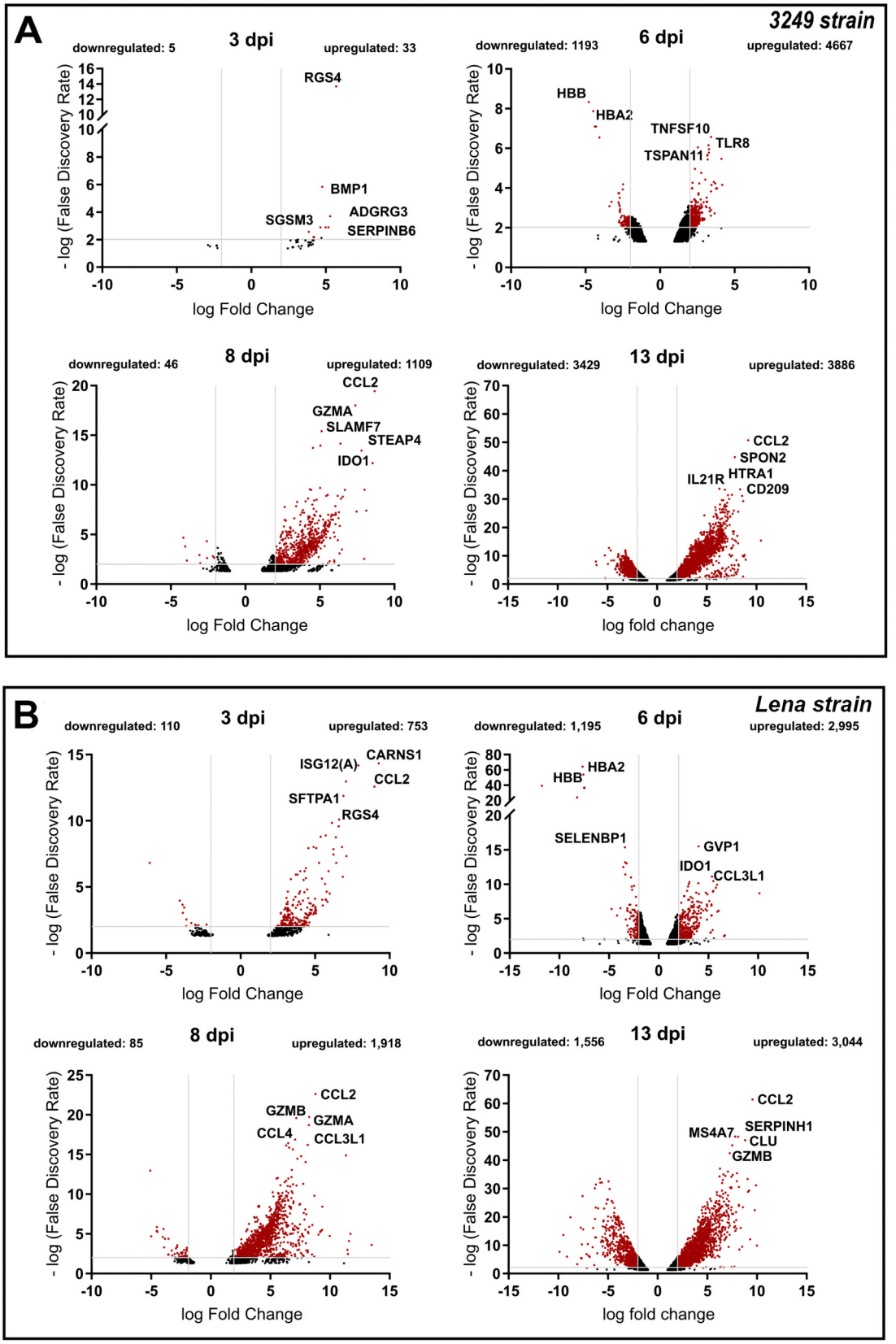

FIG 3 DEGs in 3249- (A) and Lena-infected (B) piglets MLN compared to non-infected control piglets. Volcano plots illustrate DEGs in 3249- (A) and Lena-infected (B) piglets to non-infected control piglets at different time points (3, 6, 8, and 13 dpi). Red dots show DEGs with an FDR < 0.05 and an absolute $\log_2$ fold change ≥ 1, underlining the top 5 DEGs with a higher fold change. Because of the low number of DEGs not data was showed at 1 dpi.

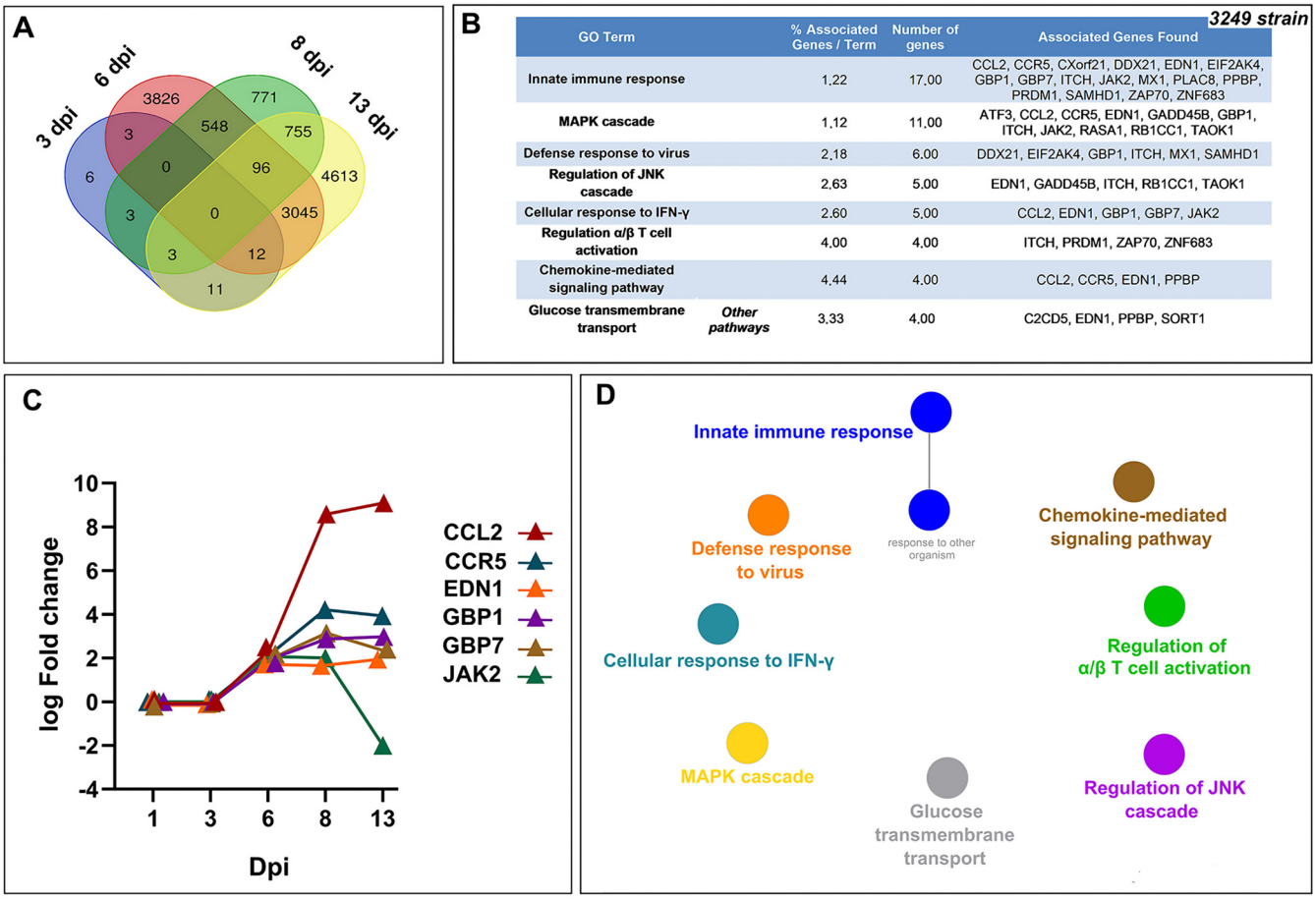

GO Term		% Associated Genes / Term	Number of genes	Associated Genes Found
Innate immune response		1,22	17,00	CCL2, CCR5, CXorf21, DDX21, EDN1, EIF2AK4, GBP1, GBP7, ITCH, JAK2, MX1, PLAC8, PPBP, PRDM1, SAMHD1, ZAP70, ZNF683
MAPK cascade		1,12	11,00	ATF3, CCL2, CCR5, EDN1, GADD45B, GBP1, ITCH, JAK2, RASA1, RB1CC1, TAOK1
Defense response to virus		2,18	6,00	DDX21, EIF2AK4, GBP1, ITCH, MX1, SAMHD1
Regulation of JNK cascade		2,63	5,00	EDN1, GADD45B, ITCH, RB1CC1, TAOK1
Cellular response to IFN-γ		2,60	5,00	CCL2, EDN1, GBP1, GBP7, JAK2
Regulation α/β T cell activation		4,00	4,00	ITCH, PRDM1, ZAP70, ZNF683
Chemokine-mediated signaling pathway		4,44	4,00	CCL2, CCR5, EDN1, PPBP
Glucose transmembrane transport	*Other pathways*	3,33	4,00	C2CD5, EDN1, PPBP, SORT1

FIG 4 Venn diagram displaying the distribution of DEGs in low-virulent 3249-infected piglets at each time point (A). Gene ontology (GO) analysis of 96 overlapped DEGs in response to 3249 strain infection at 6–8–13 dpi. Table lists the top terms of GO biological processes (BPs) and immune system processes (ISPs) enriched with 96 overlapped DEGs (B). Pattern of expression of representative genes (*CCL2*, *CCR5*, *EDN1*, *GBP1*, *GBP7*, *JAK2*) for the most relevant pathways (C). Functional network of BPs and ISPs pathways for the module were visualized in Cytoscape with ClueGo and CluePedia (D). Only the statistically significant terms (FDR $<$ 0.05) in each group are represented. Terms are displayed as nodes (filled circle) linked by edges (lines) based on their kappa value ($\geq$ 0.4), where only the label of the most significant term per group is shown.

and C, respectively, and selected as sub-networks (Fig. 7A). Interestingly, all the Hub genes identified for the 3249 strain were included in cluster A. "Positive regulation of leukocyte activation" (11 out of 20 Hub genes), "regulation of T-cell activation (11 out of 20 Hub genes) and differentiation (9 out of 20 Hub genes)," "lymphocyte migration" (5 out of 20 Hub genes), "positive regulation of α/β T-cell activation" (2 out of 20 Hub genes), "IL-2 receptor activity" (3 out of 20 Hub genes), and "tolerance induction" (3 out of 20 Hub genes) were the main terms involved after screening of GO enrichment analyses (BPs and ISPs categories) of genes included within cluster A (Fig. 7B, Table 1).

Identification and functional classification of conserved DEGs in response to virulent Lena strain infection. A sum of 11,656 DEGs were found in the Lena data set (Fig. 8A), with most of them (6,760 genes) being expressed only at one single time point during the infection. The same approach described above was followed to analyze the 3249 data set; the analysis was addressed in DEGs identified at two or more time points.

Noteworthy, 5 conserved DEGs, all of them upregulated, were identified at 1–3–6–8–13 dpi including colony-stimulating factor 1 (*CSF1*), chemokine (C-C motif) ligands 4 (*CCL4*), six-transmembrane epithelial antigen of prostate 4 (*STEAP4*), transglutaminase 2 (*TGM2*), and endothelin 1 (*EDN1*) (Fig. 8B).

At 3–6–8–13 dpi, 82 overlapped DEGs were identified among which only 3 were downregulated, whereas 79 were upregulated (Fig. 8A). In the next step, a GO functional-enrichment analysis was conducted (BPs and ISPs categories), with most of the

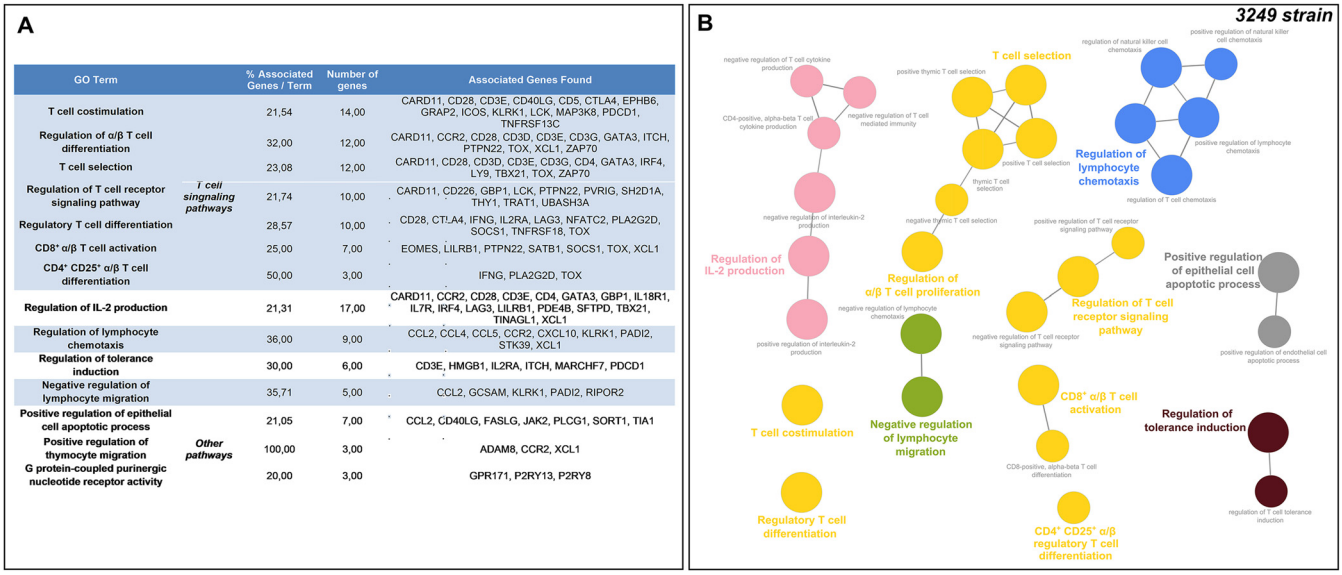

GO Term		% Associated Genes / Term	Number of genes	Associated Genes Found
T cell costimulation	*T cell singnaling pathways*	21,54	14,00	CARD11, CD28, CD3E, CD40LG, CD5, CTLA4, EPHB6, GRAP2, ICOS, KLRK1, LCK, MAP3K8, PDCD1, TNFRSF13C
Regulation of α/β T cell differentiation		32,00	12,00	CARD11, CCR2, CD28, CD3D, CD3E, CD3G, GATA3, ITCH, PTPN22, TOX, XCL1, ZAP70
T cell selection		23,08	12,00	CARD11, CD28, CD3D, CD3E, CD3G, CD4, GATA3, IRF4, LY9, TBX21, TOX, ZAP70
Regulation of T cell receptor signaling pathway		21,74	10,00	CARD11, CD226, GBP1, LCK, PTPN22, PVRIG, SH2D1A, THY1, TRAT1, UBASH3A
Regulatory T cell differentiation		28,57	10,00	CD28, CTLA4, IFNG, IL2RA, LAG3, NFATC2, PLA2G2D, SOCS1, TNFRSF18, TOX
CD8⁺ α/β T cell activation		25,00	7,00	EOMES, LILRB1, PTPN22, SATB1, SOCS1, TOX, XCL1
CD4⁺ CD25⁺ α/β T cell differentiation		50,00	3,00	IFNG, PLA2G2D, TOX
Regulation of IL-2 production		21,31	17,00	CARD11, CCR2, CD28, CD3E, CD4, GATA3, GBP1, IL18R1, IL7R, IRF4, LAG3, LILRB1, PDE4B, SFTPD, TBX21, TINAGL1, XCL1
Regulation of lymphocyte chemotaxis		36,00	9,00	CCL2, CCL4, CCL5, CCR2, CXCL10, KLRK1, PADI2, STK39, XCL1
Regulation of tolerance induction		30,00	6,00	CD3E, HMGB1, IL2RA, ITCH, MARCHF7, PDCD1
Negative regulation of lymphocyte migration		35,71	5,00	CCL2, GCSAM, KLRK1, PADI2, RIPOR2
Positive regulation of epithelial cell apoptotic process	*Other pathways*	21,05	7,00	CCL2, CD40LG, FASLG, JAK2, PLCG1, SORT1, TIA1
Positive regulation of thymocyte migration		100,00	3,00	ADAM8, CCR2, XCL1
G protein-coupled purinergic nucleotide receptor activity		20,00	3,00	GPR171, P2RY13, P2RY8

FIG 5 Gene Ontology (GO) analysis of 854 overlapped DEGs in response to 3249 strain infection at 8–13 dpi. Table lists the top terms of GO biological processes (BPs) and immune system processes (ISPs) enriched with 854 overlapped DEGs (A). Functional network of BPs and ISPs pathways for the module were visualized in Cytoscape with ClueGo and CluePedia (B). Only the statistically significant terms (FDR < 0.05) in each group are represented. Terms are displayed as nodes (filled circle) linked by edges (lines) based on their kappa value (≥ 0.4), where only the label of the most significant term per group is shown.

DEGs enriched in terms associated with "IFN-I signaling pathway" (8 DEGs, 19.05%), "neutrophil migration" (7 DEGs, 16.78%), "negative regulation of T-cell mediated cytotoxicity" (3 DEGs, 7.14%) and "negative regulation of $CD8^+$ α/β T cell activation" (3 DEGs, 33.33%). Fig. 9 lists the symbol and number of genes enriched in each GO term, as well as the patterns of expression of representative genes for the virulent Lena strain (Fig. 9B).

Consequently, a sum of 332 overlapped DEGs was disclosed at 6–8–13 dpi, most of them (311) upregulated with only 21 genes downregulated (Fig. 8B). In this case, according to the GO functional-enrichment analysis (BPs and ISPs categories), the majority of DEGs were significantly enriched within "IFN-I signaling pathway" (11 DEGS, 14.67%) and T-cell signaling pathways (11 DEGs, 16.10%) (Fig. 10). Moreover, other highly enriched GO terms were identified, underlining "positive regulation of lymphocyte migration" (6 DEGs, 8.00%), "tolerance induction to lipopolysaccharide" (6 DEGs, 8.00%), "regulation of IFN-γ-mediated signaling pathway" (5 DEGs, 6.67%), and "regulation of chronic response" (5 DEGs, 6.67%). Fig. 10 lists the symbol and number of genes enriched in each GO term.

Finally, a total of 1,227 overlapped genes were differentially expressed at 8–13 dpi, which included 48 downregulated and 1,179 upregulated genes (Fig. 8B). After screening of GO enrichment analysis, T-cell signaling pathways were found to be highly impaired, with 138 DEGs (32.43%) enriched in 9 different GO terms (Fig. 11). In addition, we found further significant enriched GO terms such as "lymphocyte chemotaxis" (30 DEGs, 6.9%), "regulation of IFN-γ production" (27 DEGs, 6.21%), "chemokine-mediated signaling pathway" (25 DEGs, 5.75%), "NK cell mediated immunity" (18 DEGs, 4.14%), "regulation of vitamin D biosynthetic process" (12 DEGS, 44.44%), "positive regulation of leukocyte apoptotic process" (8 DEGs, 2.07%), and "regulation of tolerance induction" (7 DEGs, 1.61%). Fig. 11 and Table 2 list the symbol and number of genes enriched in each GO term.

PPI network construction and Hub genes identification for virulent Lena infection. In this case, the 1,227 overlapped DEGs detected at 8–13 dpi were utilized to construct the PPI network by the STRING database, finding 560 nodes and 4,461 edges. Afterwards, according to the MCC and DMNC algorithm of the CytoHubba plugin, the top 10 highest-scored genes found for each approach from the whole PPI

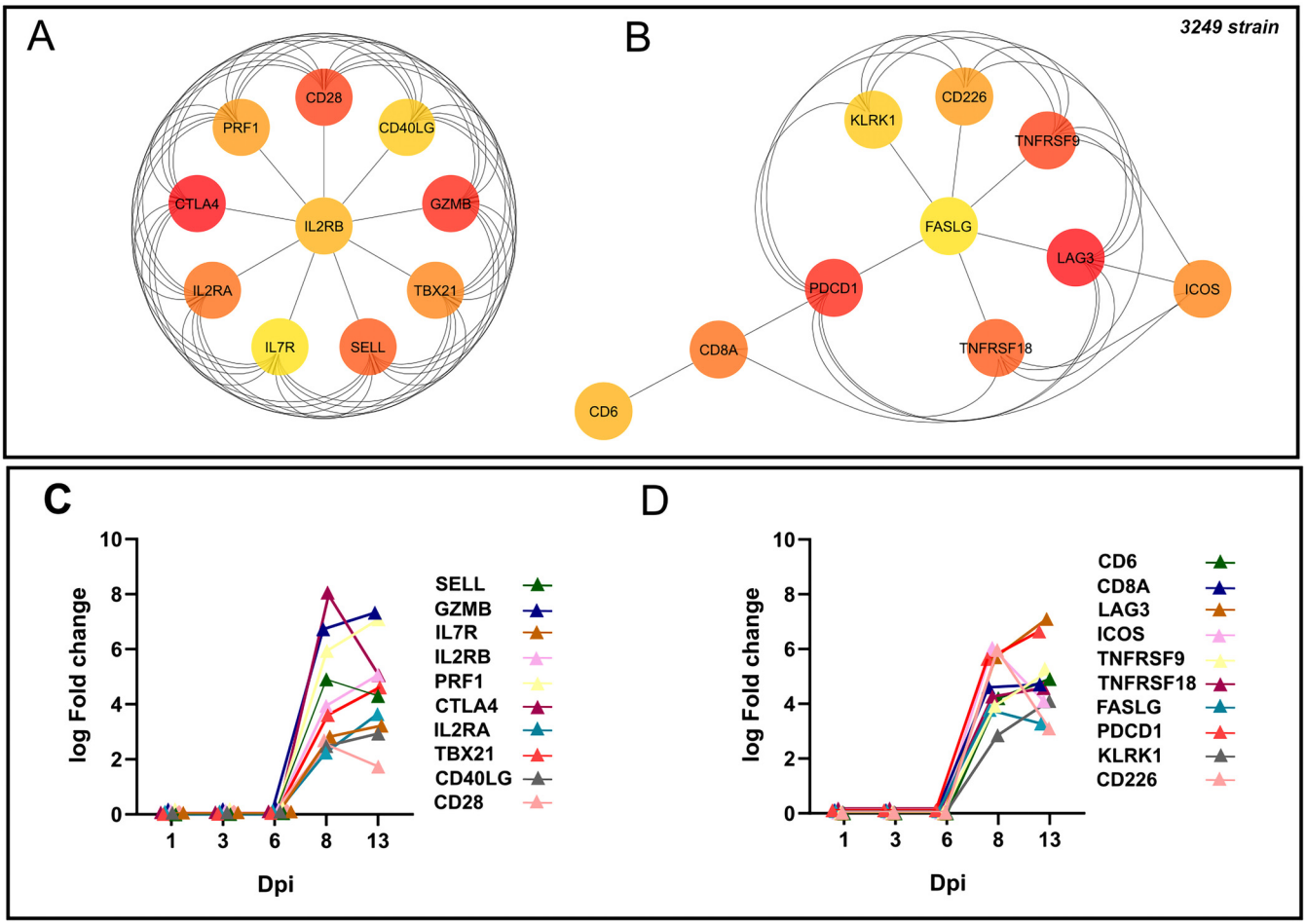

FIG 6 Hub genes network for low-virulent 3249 strain. Hub genes for 3249 strain were disclosed according to Maximal Clique Centrality (MCC) (A), and Density of Maximum Neighborhood Component (DMNC) (B) algorithms were identified from the whole PPI network. Kinetic of expression of Hub genes for 3249 strain along the infection (C and D). The fold change for each Hub gene was illustrated as the median of the group at 1, 3, 6, 8, and 13 dpi.

network were identified as Lena strain Hub genes, highlighting *CTLA4*, *CCR7*, *SELL*, *CD28*, *CD274*, *IL-10*, *GZMB*, *TBX21*, *CD40LG*, *CD27*, *LAG3*, *PDCD1*, *HAVCR2*, *ICOS*, *TNFRSF18*, *TNFRSF4*, *TNFRSF9*, *GPR18*, *CD1D* and *CD226* (Fig. 12A and B). The kinetics of expression Hub genes disclosed for the virulent Lena strain was displayed in Fig. 12C and D. Of note, several of these Lena strain Hub genes (11 out of 20) were previously identified for the 3249 strain. After analyzing the whole PPI network by MCODE plugin, the top 3 more significant sub-networks were selected and named as cluster A, cluster B, and cluster C (Fig. 13A). Cluster A, which included most of Lena strain Hub genes, was subsequently subjected to a GO functional-enrichment analysis (BPs and ISPs categories). "Regulation of lymphocyte apoptotic process" (4 out of 20 Hub genes), "T-cell selection" (7 out of 20 Hub genes), "positive regulation of IL-4 production" (5 out of 20 Hub genes), "T-cell co-stimulation" (5 out of 20 Hub genes), "regulation of tolerance induction" (4 out of 20 Hub genes), "regulation of IL-2 production" (4 out of 20 Hub genes), "regulation of regulatory T-cell differentiation" (4 out of 20 Hub genes), "regulation of lymphocyte chemotaxis," and "regulation of IFN-α production" (2 out of 20 Hub genes) were reported as highly enriched GO terms (Fig. 13B, Table 3).

Verification of the DEGs expression patterns and Hub genes by RT-qPCR. Twelve Hub genes (*CCR7*, *CD274* (PDL-1), *CD28*, *CTLA4*, *GZMB*, *HACVR2* (TIM3), *IL-10*, *LAG3*, *SELL*, *TBX21* (T-BET), *PDCD1* (PD-1), *TNFRSF9* (CD137)) found either in the Lena or 3249 group were arbitrarily selected to confirm their differential expression levels by RT-qPCR. As shown in Table 4, the qPCR results of the Hub genes agreed with those of RNA-seq analysis, validating the RNA-seq data herein reported.

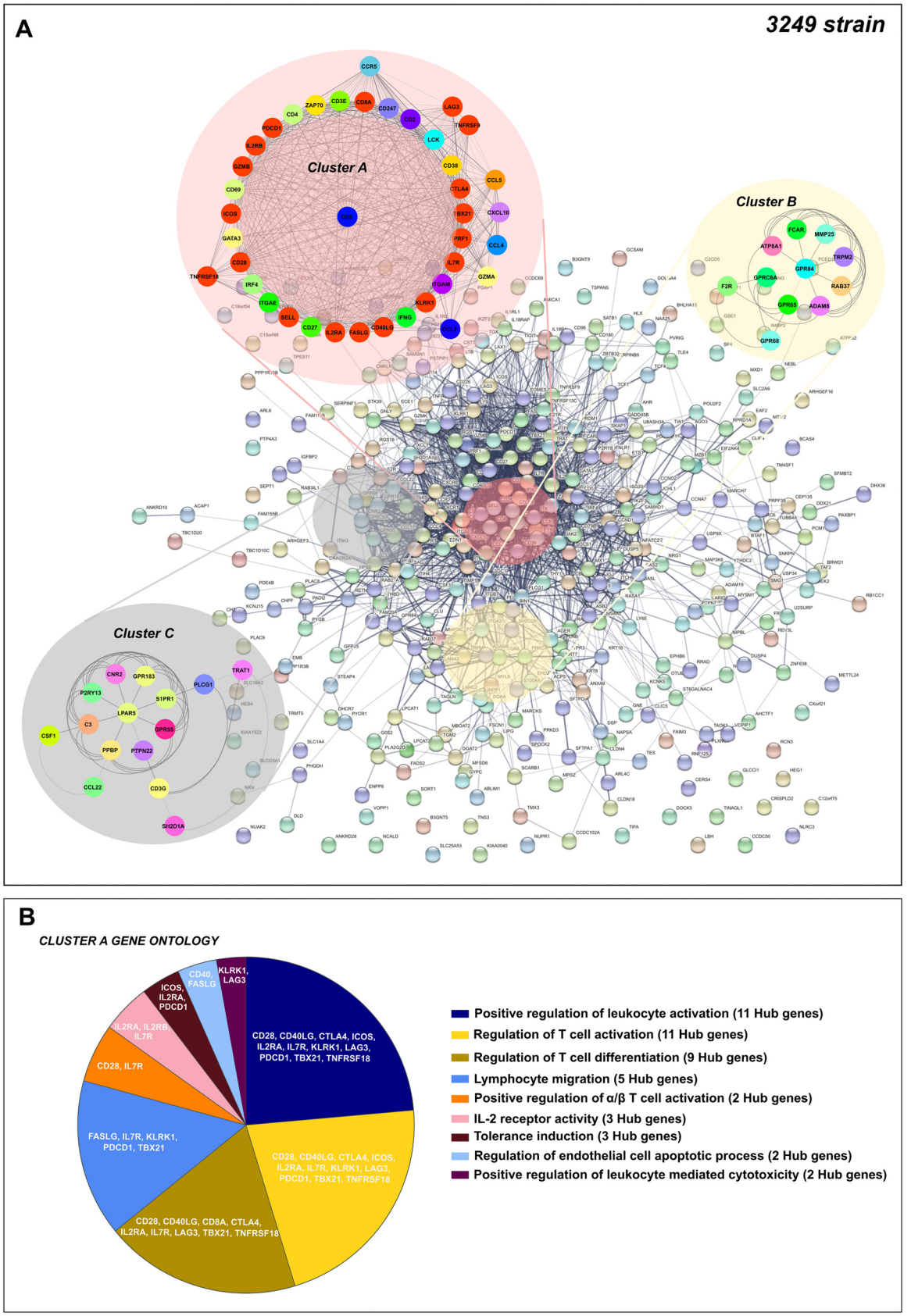

FIG 7 PPI network of 854 overlapped DEGs in response to 3249 strain infection at 8–13 dpi (A). Network was constructed by STRING database and visualized by Cytoscape, underlining the significant clusters A, B, and C (κ-core $>$ 6), which were identified by means of

(Continued on next page)

TABLE 1 Gene Ontology (GO) analysis of Cluster A DEGs in response to 3249 strain infection at 8–13 dpi

GO term	% associated genes/term	No. of genes	Associated genes found
Positive regulation of leukocyte activation	5.01	25,00	CCL2, CCL5, CD2, CD27, CD28, CD38, CD3E, CD4, CD40LG, CD5, CTLA4, GATA3, ICOS, IFNG, IL2RA, IL7R, IRF4, ITGAM, KLRK1, LAG3, LCK, PDCD1, TBX21, TNFRSF18, ZAP70
Regulation of T cell activation	6.55	23,00	CCL2, CCL5, CD2, CD27, CD28, CD3E, CD4, CD40LG, CD5, CTLA4, GATA3, ICOS, IFNG, IL2RA, IL7R, IRF4, KLRK1, LAG3, LCK, PDCD1, TBX21, TNFRSF18, ZAP70
Regulation of T cell differentiation	8.50	20,00	CCL5, CD2, CD247, CD27, CD28, CD3E, CD4, CD40LG, CD8A, CTLA4, GATA3, IFNG, IL2RA, IL7R, IRF4, LAG3, LCK, TBX21, TNFRSF18, ZAP70
Lymphocyte migration	6.61	16,00	CCL2, CCL4, CCL5, CCR5, CD27, CD3E, CD4, CXCL10, FASLG, GATA3, IFNG, IL7R, KLRK1, PDCD1, TBX21, ZAP70
Positive regulation of α/β T cell activation	6.06	6,00	CD28, CD3E, GATA3, IFNG, IL7R, ZAP70
IL-2 receptor activity	66.67	5,00	CCR5, CD4, IL2RA, IL2RB, IL7R
Tolerance induction	14.29	4,00	CD3E, ICOS, IL2RA, PDCD1
Regulation of endothelial cell apoptotic process	7.84	4,00	CCL2, CD40LG, FASLG, GATA3
Positive regulation of leukocyte mediated cytotoxicity	5.08	3,00	ITGAM, KLRK1, LAG3

DISCUSSION

PRRSV have evolved different mechanisms to evade the host's immune response (18, 20), favoring also secondary infections that result in severe disease such as PRDC (23). Understanding the mechanisms involved in the dysregulation of the immune response at lung level is a cornerstone for unraveling the immunopathogenesis of PRRS, one of the most economically devastating diseases for swine production.

Time-series analysis pointed out an early and sustained upregulation of co-inhibitory receptors related to T-cell and NK cell functions over time points. In the present study, RNA-seq was used to perform a time course analysis in BAL cells upon PRRSV *in vivo* infection with strains of different virulence to gain further insight into the potential pathways involved in modulating the host's immune response. Clusters 3, 4, and 5 consisted of genes whose expression levels increased during the time course, although with different patterns and intensity for each strain. Genes in cluster 3, which exhibited a similar kinetics to lung lesion, were enriched in the GO terms "regulation of immune system process," "leukocyte differentiation," "regulation of cytokine production," "lymphocyte activation," and "response to cytokine and positive regulation of apoptotic process," among others. These terms related to viral infection and immune response signaling pathways were upregulated earlier and higher in virulent Lena-infected than in low-virulent 3249-infected piglets, which may explain the severe lung injury observed. In addition, a group of genes was enriched for "negative regulation of immune system process" (Fig. 2A), including *CD96*, *CTLA4*, *RFN128*, *TIGIT*, and *SAMHD1*, which play an inhibitory role in T-cell and NK cell functions (33–38), potentially hampering viral clearance and the onset of an effective adaptive immune response.

Cluster 4 included genes that were strongly and promptly upregulated in virulent Lena-infected compared with low-virulent 3249-infected piglets. GO terms such as "cytokine-mediated signaling pathway," "response to bacterium," "regulation of cytokine production," "IFN-I signaling pathway," and "cellular response to tumor necrosis factor" were enriched in this cluster. According to our previous results and those from others, these inflammatory-

FIG 7 Legend (Continued)

MCODE. The genes calculated by Maximal Clique Centrality (MCC) and Density of Maximum Neighborhood Component (DMNC) algorithms were selected as Hub genes (genes with the highest degree of connectivity) by CytoHubba plugin in Cytoscape. Most of the Hub genes (red color) were included in cluster 1. GO enrichment analysis (biological processes, BPs, and immune system processes, ISPs, categories) of DEGs included within cluster A (B). Overview pie chart shows the proportion of genes associated with the top functional groups, indicating the name of Hub genes in each term. Table 1 lists the top terms of GO (BPs and ISPs).

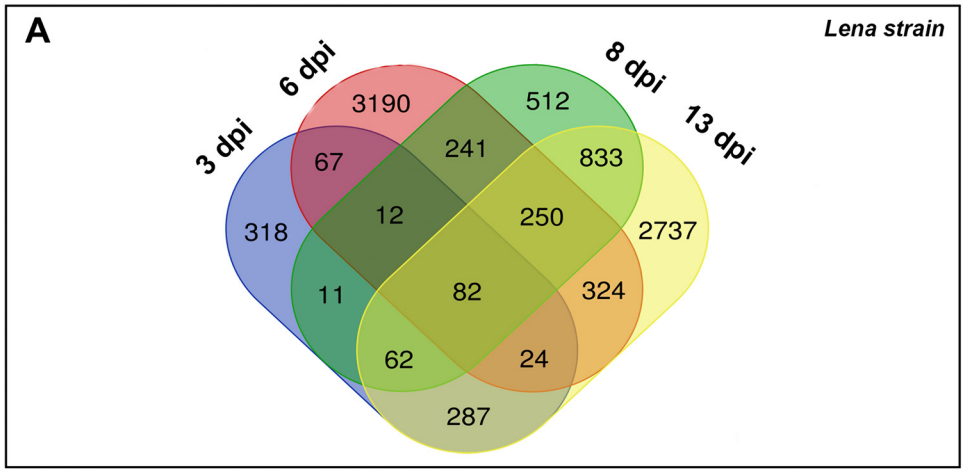

B

Genes	Proteins	Description
TGM2	Protein-glutamine γ-glutamyltransferase 2	Catalyzes the cross-linking of proteins and the conjugation of polyamines to proteins
EDN1	Preproendothelin 1	Endothelins are endothelium-derived vasoconstrictor peptides
CSF1	Colony stimulating factor 1	Cytokine that plays an essential role in the regulation of survival, proliferation and differentiation of hematopoietic precursor cells, especially mononuclear phagocytes, such as macrophages and monocytes. Promotes the release of proinflammatory chemokines, and thereby plays an important role in innate immunity and in inflammatory processes.
STEAP4	Six-transmembrane epithelial antigen of prostate 4	Metalloreductase that has the ability to reduce both Fe(3+) and Cu(2+). Plays a role in systemic metabolic homeostasis, integrating inflammatory and metabolic responses.
CCL4	Macrophage inflammatory protein 1β	Monokine with inflammatory and chemokinetic properties. Binds to CCR5.

FIG 8 Table lists 5 upregulated DEGs conserved in response to virulent Lena infection at 1–3–6–8–13 dpi (A). Venn diagram displaying the distribution of DEGs in virulent Lena-infected piglets at each time point (B).

related pathways contribute to the severe clinical outcomes and lung lesions observed in Lena-infected piglets, but also to an early upregulation of pro-inflammatory cytokines associated with a high viral load and the induction of regulated cell death (14, 39–42). These results confirm that the dynamics and extent of virulent Lena strain replication are critical for the disease outcome, inducing a strong and early inflammatory response in the lung.

On the other hand, cluster 5 genes involved the GO terms "lipid transport" and "carboxylic acid transport," whose expression increased in parallel in both PRRSV-1-infected groups from 8 to 13 dpi. Viruses are able to exploit cellular lipid transport, signaling, and metabolism for their own advantage, making viral entry, replication, or assembly of virions easier (43). DEGs associated with lipid signaling pathways have already been described during PRRSV infection, suggesting that PRRSV strains could modify host's cells lipid metabolism to enable either viral replication or virion release (24, 26).

The interplay among IFN-I/IFN-II orchestrated an antiviral response resulting in IFN-stimulated genes unable to control efficiently viral replication, probably due to PRRSV countermeasures. IFN-I leads to a signal transduction cascade of hundreds of IFN-stimulated genes (ISGs), a powerful instrument that interferes with viral replication (44, 45). In our case, a screen of ISGs, enriched in IFN-I signaling pathway, was upregulated in BAL cells from both virulent Lena-infected (*BST2*, *IFI6*, *IFITM1*, *ISG15*, *ISG20*, *MX1*, *OASL*, *RSAD2*, *STAT1*) and low-virulent 3249-infected piglets (*EIF2AK4*, *GBP1*, *MX1*) from 3 and 6 dpi onwards, respectively. Interferon regulatory factors (IRF) have been also found to be overexpressed in PAMs infected *in vitro* with Lena and Lelystad virus strains (29), as well as during the early stage of PRRSV-2 infection (24, 46, 47). Many of these upregulated genes could point to a continuous antiviral state (45, 48), since *ISG20*, *MX1*, and *RSAD2* have the capacity to inhibit viral replication (49–51), nevertheless, PRRSV has been

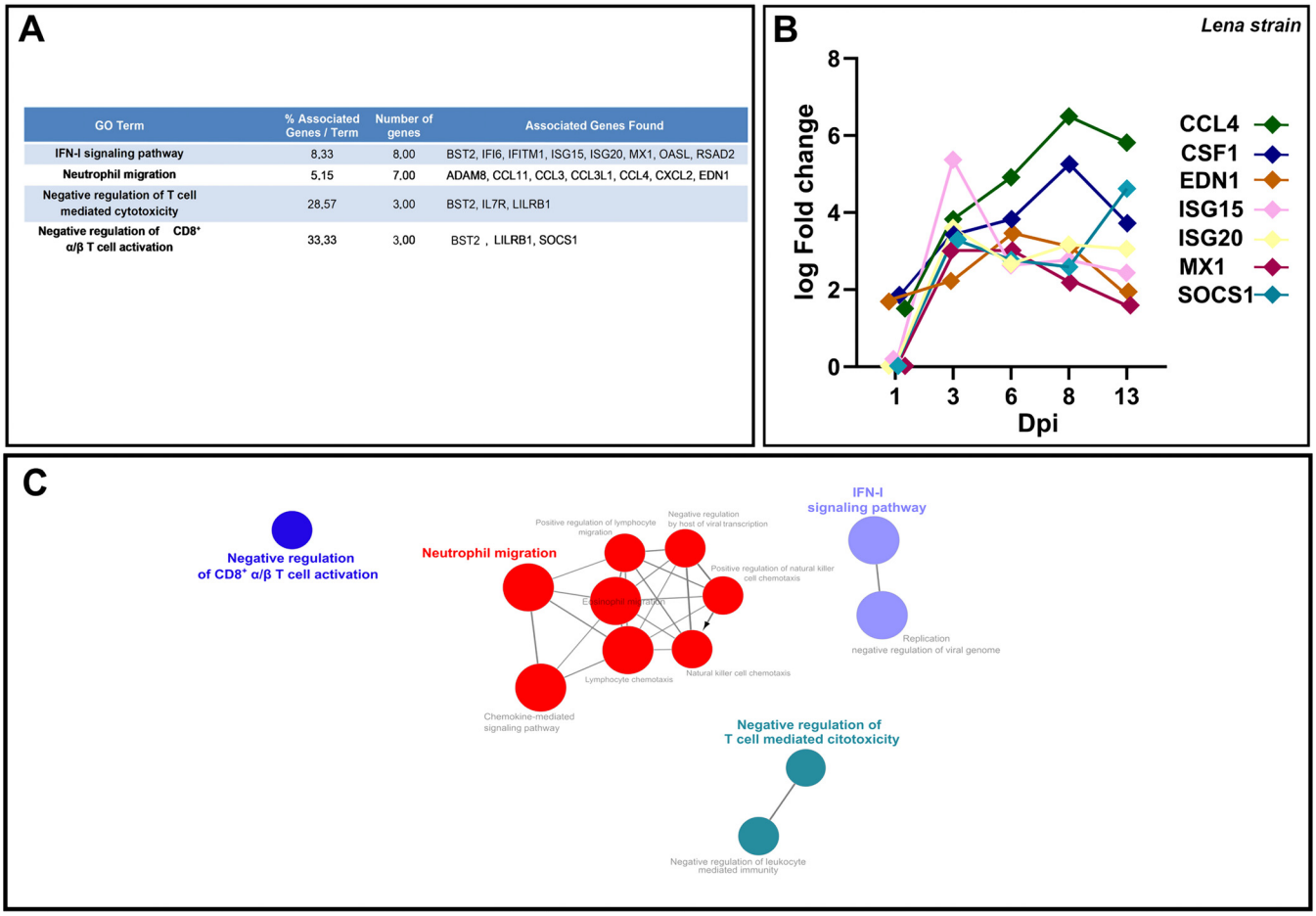

FIG 9 Gene Ontology (GO) analysis of 82 overlapped DEGs in response to Lena strain infection at 3–6–8–13 dpi. Table lists the top terms of GO biological processes (BPs) and immune system processes (ISPs) enriched with 82 overlapped DEGs (A). Pattern of expression of representative genes (*CCL4*, *CSF1*, *EDN1*, *ISG15*, *ISG20*, *MX1*, *SOCS1*) for the most relevant pathways (B). Functional network of BPs and ISPs pathways for the module were visualized in Cytoscape with ClueGo and CluePedia (C). Only the statistically significant terms (FDR $<$ 0.05) in each group are represented. Terms are displayed as nodes (filled circle) linked by edges (lines) based on their kappa value ($\geq$ 0.4), where only the label of the most significant term per group is shown.

reported to inhibit *IRF3* as well as several of these ISGs such as *STAT1*, *ISG15*, and *IFITM1* (52, 53), by viral non-structural proteins (nsp1α, nsp1β, nsp2, nsp4, and nsp11) (53–56). Thus, unlike the 3249 strain, the virulent Lena strain induced an upregulation of DEGs enriched in negative regulation of IFN-I and type II IFN (IFN-II) at 8–13 dpi in our study. Altogether, these results draw an interplay among IFN-I/IFN-II induced antiviral response and PRRSV countermeasures resulting in ISGs unable to control efficiently viral replication, leading to an incomplete viral clearance and potential persistent infection (57).

Early upregulation of chemokines and cytokines in response to virulent Lena infection led to an acute lung injury. Virulent PRRSV-1 strains trigger an exacerbated and early pro-inflammatory response compared with low-virulent strains, leading to severe lung injury, secondary bacterial infection, and hence, acute respiratory symptoms (12, 39, 58, 59). A considerable number of DEGs were enriched in GO terms involved in macrophages activation, pro- and anti-inflammatory cytokines, as well as chemokines for the recruitment of neutrophils, monocytes, and lymphocytes to the site of infection in both PRRSV-1-infected groups during the study. Interestingly, Lena-infected pigs showed 5 DEGs, which were upregulated from 1 to 13 dpi, with three of them (*CSF1*, *CCL4*, and *EDN1*) showing striking inflammatory properties, such as monocyte and macrophage proliferation and differentiation (*CSF1*) (60), vasoconstriction and pro-inflammatory response associated with acute lung injury (ALI) (*EDN1*) (61), or neutrophil migration (*CCL4*) (62). Although, PAMs are the key players during PRRSV infection, the GO analysis suggests that chemotaxis of neutrophils and their likely

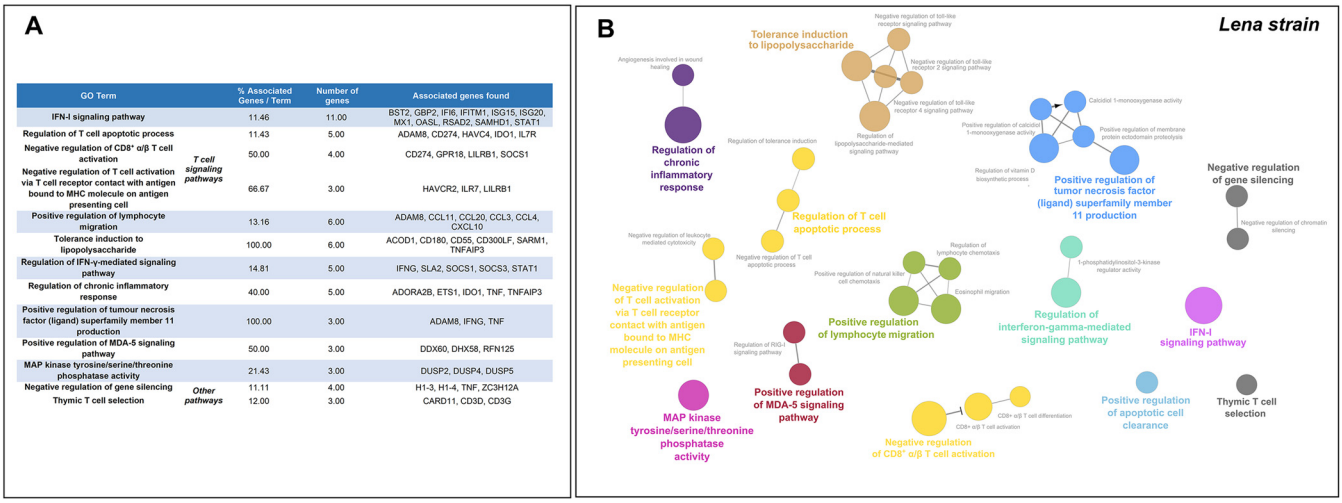

GO Term		% Associated Genes / Term	Number of genes	Associated genes found
IFN-I signaling pathway		11.46	11.00	BST2, GBP2, IFI6, IFITM1, ISG15, ISG20, MX1, OASL, RSAD2, SAMHD1, STAT1
Regulation of T cell apoptotic process		11.43	5.00	ADAM8, CD274, HAVC4, IDO1, IL7R
Negative regulation of CD8+ α/β T cell activation	*T cell signaling pathways*	50.00	4.00	CD274, GPR18, LILRB1, SOCS1
Negative regulation of T cell activation via T cell receptor contact with antigen bound to MHC molecule on antigen presenting cell		66.67	3.00	HAVCR2, IL7R, LILRB1
Positive regulation of lymphocyte migration		13.16	6.00	ADAM8, CCL11, CCL20, CCL3, CCL4, CXCL10
Tolerance induction to lipopolysaccharide		100.00	6.00	ACOD1, CD180, CD55, CD300LF, SARM1, TNFAIP3
Regulation of IFN-γ-mediated signaling pathway		14.81	5.00	IFNG, SLA2, SOCS1, SOCS3, STAT1
Regulation of chronic inflammatory response		40.00	5.00	ADORA2B, ETS1, IDO1, TNF, TNFAIP3
Positive regulation of tumour necrosis factor (ligand) superfamily member 11 production		100.00	3.00	ADAM8, IFNG, TNF
Positive regulation of MDA-5 signaling pathway		50.00	3.00	DDX60, DHX58, RFN125
MAP kinase tyrosine/serine/threonine phosphatase activity		21.43	3.00	DUSP2, DUSP4, DUSP5
Negative regulation of gene silencing	*Other pathways*	11.11	4.00	H1-3, H1-4, TNF, ZC3H12A
Thymic T cell selection		12.00	3.00	CARD11, CD3D, CD3G

FIG 10 Gene Ontology (GO) analysis of 332 overlapped DEGs in response to Lena strain infection at 6–8–13 dpi. Table lists the top terms of GO biological processes (BPs) and immune system processes (ISPs) enriched with 332 overlapped DEGs (A). Functional network of BPs and ISPs pathways for the module was visualized in Cytoscape with ClueGo and CluePedia (B). Only the statistically significant terms (FDR $<$ 0.05) in each group are represented. Terms are displayed as nodes (filled circle) linked by edges (lines) based on their kappa value ($\geq$ 0.4), where only the label of the most significant term per group is shown.

degranulation are continued over the time points (25, 46), leading to alveolar–capillary barrier damage, increased vascular permeability, and hence, a higher extent of lung damage, as has been observed in this study.

According to the dynamic changes observed in BAL cells from PRRSV-1-infected piglets, the "positive regulation of lymphocyte migration" term was observed in virulent Lena-infected piglets from 6 dpi onwards, including upregulated expression of *ADAM8*, *CCL11*, *CCL20*, *CCL3*, *CCL4*, and *CXCL10*. By contrast, in the 3249 group not only were these genes overexpressed later (8-13 dpi), but also, genes enriched in "negative regulation of lymphocyte migration" were found (*CCL2*, *GCSAM*, *KLRK1*, *PADI2*, *RIPOR2*). *CCL20/MIP-3*α is a strong chemotactic factor for lymphocytes, while a weak factor for neutrophils, that is upregulated by IFN-γ, tumor necrosis factor (TNF) and lipopolysaccharide, inducing a marked lung damage upon viral infection (63). *CCL2*, *CCL3*, *CCL4*, and *CCXL10* are produced in the lung in the early phase of lung inflammation, working as a chemotactic factor for macrophages, NK cells, and T cells during viral infection (64). In addition, there was an upregulation of genes associated with "positive regulation of apoptotic cell clearance" (*C3*, *C4*, *CD300LF*, *CCL2*) in Lena-infected piglets from 6 to 13 dpi, probably, due to the severe activation of regulated cell death phenomena at lung level induced by the virulent Lena strain (42), suggesting an attempt to remove dead cells and cellular debris to restore tissue damage.

Interestingly, many cytokine-signaling pathways were found to be regulated in Lena- compared with 3249-infected piglets, highlighting an interplay among pro- and anti-inflammatory responses that are likely to be activated in a virulence dependent fashion and hence influencing the profile of innate cytokines as well as the development of adaptive immunity. IFN-γ release pathway was observed in the 3249 group from 6 dpi onwards, whereas *SOCS1* and *SOSC3*, potent IFN-γ inhibitors (65), were early overexpressed in the Lena group (6 dpi) followed by an interface of upregulated genes that may promote IFN-γ production (8–13 dpi). *IL1B* (IL-1β) and *TNF* genes were upregulated in the Lena group, unlike the 3249 group. While classical PRRSV strains are reported to show a delayed and weak systemic production of these cytokines (66–69), this proinflammatory profile seems to be a hallmark of virulent PRRSV strains (24, 25, 39, 58, 59), resulting in being useless in controlling viral replication but exacerbating clinical signs and lung damage.

Moreover, the virulent Lena strain induced a strong regulation of adaptive-cytokines-related pathways such as "regulation of IL-2, IL-4, and IL-12 production," as well as an upregulation of *IL-10* (IL-10) and *IL18BP* (IL-18BP, IL-18 binding protein) from 8 to

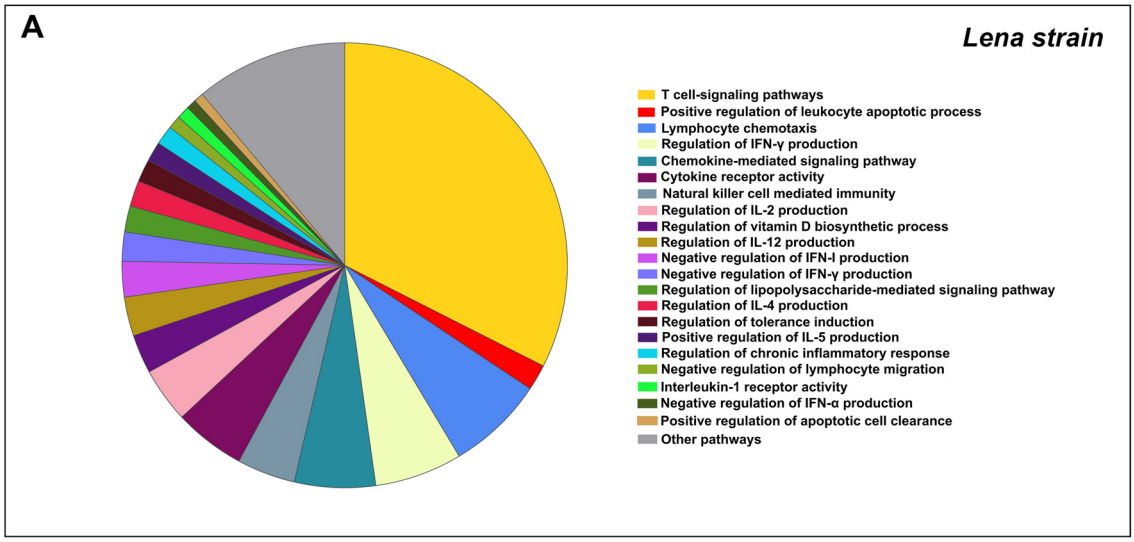

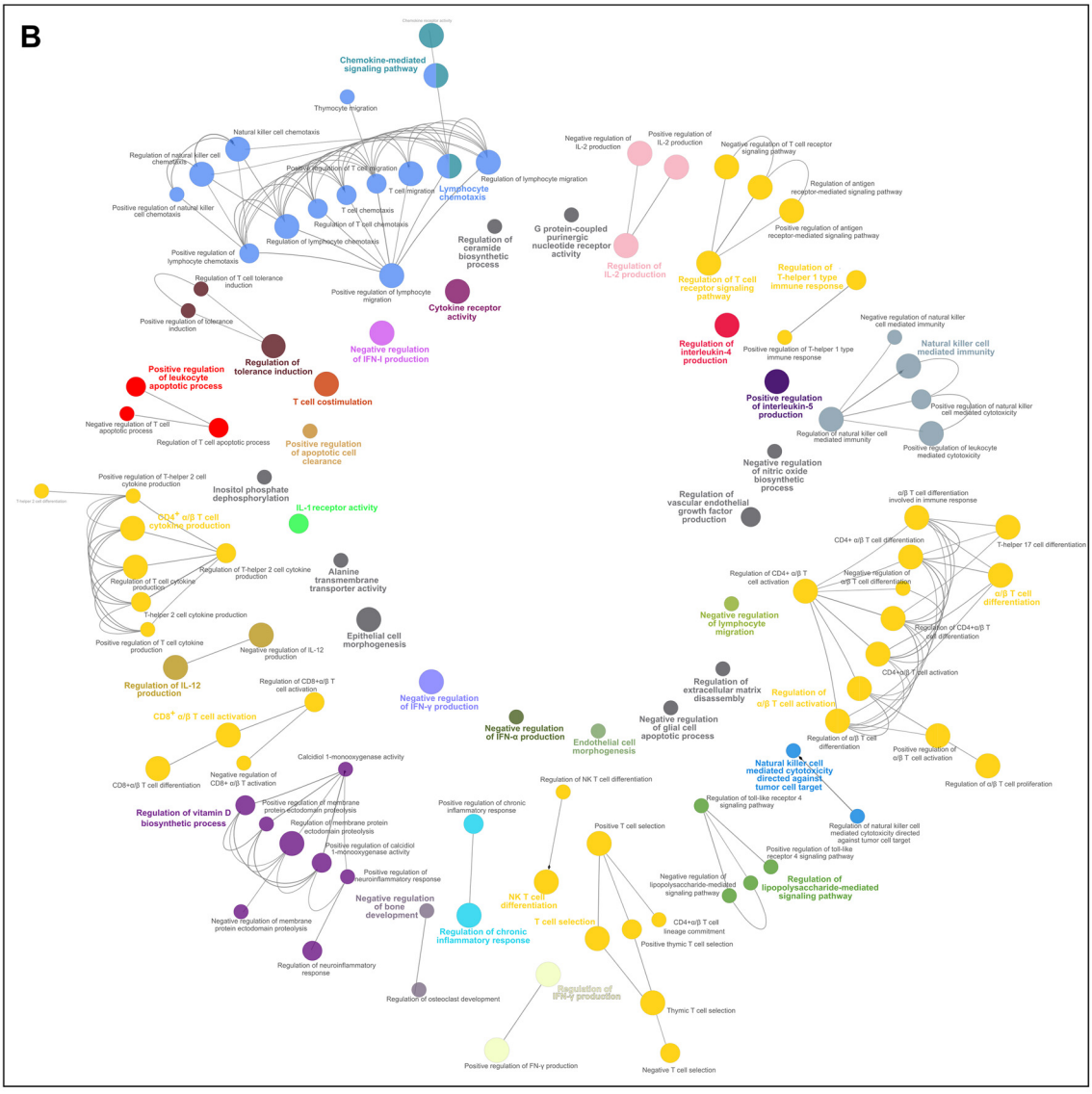

FIG 11 Gene Ontology (GO) analysis of 1,227 overlapped DEGs in response to Lena strain infection at 8–13 dpi. Overview pie chart illustrates the top terms of GO biological processes (BPs) and immune system processes (ISPs) enriched with 1,227 overlapped

(Continued on next page)

13 dpi, in contrast to the 3249 group, in which only "regulation of IL-2 production" was found. Most of the genes enriched in "regulation of IL-12 production" (7 out of 12), such as *IL-10* and *IDO1*, show a negative regulation of this pathway. Likewise, upregulation of *IL-10* expression has been reported to impair Th1 response during PRRSV infection, inducing a niche for viral-specific regulatory T cells (Tregs) in a strain-dependent fashion, though Tregs induction after PRRSV infection is controversial (70–72). Although no changes in the serum concentration of IL-10 were observed in Lena- and 3249-infected pigs (41), IL-10 could be locally secreted in the lung, exerting a paracrine *in situ* effect. *IL18BP* gene encodes a soluble receptor that hijacks IL-18, blocking the engagement of IL-18 to its receptor, which in turn inhibits IL-18-induced IFN-γ production and alters Th1 response (73, 74). The anti-inflammatory mediators herein reported may play a double-edged sword role, limiting the inflammatory response during the early stage of the infection but also, when sustained in time, weakening the host's immune response against PRRSV and hence impairing viral clearance.

Activation of T-cell signaling pathways was overlapped in virulent and low-virulent PRRSV-1 strains in a time-dependent manner. Activation of T-cells is crucial for anti-PRRSV adaptive immunity since T cells are key players in tackling viral infection, particularly, during the first stages of infection (17, 75). The virulent Lena strain caused a prompt upregulation of genes enriched in "negative regulation of T cell mediated cytotoxicity," "negative regulation of CD8$^+$ α/β T-cell activation," "negative regulation of T-cell activation via T-cell receptor contact with antigen bound to MHC molecules on antigen presenting cells," and "regulation of T cell apoptotic process," which would impair the induction of CD8$^+$ cytotoxic T lymphocytes (CTLs) needed to eliminate virus-infected cells, release of pro-inflammatory cytokines, and establish memory cells (18, 75). Besides, genes associated with "regulation of chronic inflammatory response" were found to be overexpressed, suggesting that virulent Lena strain would be able to overcome the host's antiviral strategies, inducing a persistent infection. Thus, many of these DEGs (*SOCS1*, *LILRB1* (CD85J), *CD274* (PD-L1), *HAVCR2* (TIM3), and *IDO1*) enriched in the above-mentioned pathways are immune checkpoints associated with other persistent viral infections inducing T-cell exhaustion (33, 76, 77). On the other hand, a substantial number of genes were regulated from 8 dpi onwards in either Lena- or 3249-infected groups, and these DEGs were enriched in quite similar T-cell-related pathways, highlighting "T-cell co-stimulation," "T-cell selection," "regulation of α/β T-cell differentiation," and "CD8$^+$ α/β T-cell activation." T-cell stimulation is an essential mechanism that relies on co-stimulatory and co-inhibitory receptors to achieve an effective T-cell activation (78). Several viruses involved in persistent infections exploit these adaptive mechanisms to evade immune-mediated viral clearance, leading to viral persistence and, hence, a functionally inferior T-cell response (33, 79). Thereby, either Lena or 3249 elicited an upregulation of co-stimulatory receptors (*CD28*, *ICOS*, *CD40LG* (CD154), *CD27*, *TNFRSF4* (OX40), *TNFRSF9* (CD137) or *TNFRSF18* (GITR)) but also inhibitory receptors (*CD5*, *CTLA4*, *CD274* (PD-L1)/*PDCD1*, *HAVCR2* (TIM3), *LAG3*, *TIGIT*, *TOX*), some of which were also overexpressed in the thymus of these animals (80), suggesting an attempt to hamper T-cell activation. The transcription factors *GATA3* and *TBX21* (T-bet), overexpressed in both low-virulent 3249 and virulent Lena infected groups, have been reported to be involved in T-cell maturation and Th1 polarization of porcine alpha-beta T-cells (81); however, *EOMES*, upregulated as well, and *TBX21* could also cooperate to sustain exhausted CD8$^+$ T-cell subsets (78, 82, 83). Besides, we found a profile of upregulated DEGs enriched in "regulation of chronic inflammatory response" (*ADORA2B*, *CCL5*, *1001*, *IL-10*, *TNF*, *TNFAIP3*) and "regulation of tolerance induction" (*CD274*, *CD3E*, *HAVCR2*, *1001*, *IL2RA*, *MARCHF7*, *PDCD1*). Considering all the above-mentioned, two different scenarios could be drawn. First, these pathways regulate self-tolerance, minimizing bystander tis-

FIG 11 Legend (Continued)
DEGs, indicating the proportion of genes associated with each term (A). Functional network of BPs and ISPs pathways for the module were visualized in Cytoscape with ClueGo and CluePedia (B). Only the statistically significant terms (FDR $<$ 0.05) in each group are represented. Terms are displayed as nodes (filled circle) linked by edges (lines) based on their kappa value ($\geq$ 0.4), where only the label of the most significant term per group is shown. Table 2 lists the top terms of GO (BPs and ISPs).

TABLE 2 Table lists the top terms of GO biological processes (BPs) and immune system processes (ISPs) enriched with 1,227 overlapped DEGs in response to Lena strain infection at 8–13 dpi

GO term	% associated genes/term	No. of genes	Associated genes found
T cell signaling pathways			
α/β T cell differentiation	25.23	37.00	AGER, 8CL118, CCR2, CD274, CD28, CD3E, CD55, CRTAM, EBI3, EOMES, GATA3, GPR18, GPR183, HLX, IFNG, IL18R1, IRF4, ITK, LY9, NFK81Z, NLRP3, PRDM1, PTPN22, RORA, RSAD2, RUNX3, SAT81, SFTPA1, SOCS1, T8 × 21, TCF7, TOX, ZAP70, ZBT816, ZC3H12A, ZFPM1, ZNF683
Regulation of α/β T cell activation	24.00	24.00	AGER, CCR2, CD274, CD28, CD3E, CD55, CRTAM, E8I3, GATA3, HLX, IFNG, IRF4, LILR81, NFK8IZ, NLRP3, PRDM1, PTPN22, RUNX3, SOCS1, T8 × 21, ZAP70, Z8T816, ZC3H12A, ZNF683
T cell selection	32.69	17.00	8CL 118, CARD11, CCR7, CD1D, CD28, CD3D, CD3E, CD3G, CD4, GATA3, IRF4, LY9, T8 × 21, THEMIS, TOX, ZAP70, ZFPM1
T cell co-stimulation	23.08	15.00	CARD11, CCR7, CD274, CD28, CD3E, CD40LG, CDS, CTLA4, EPH86, GRAP2, ICOS, KLRK1, LCK, MAP3K8, PDCD1
Regulation of T cell receptor signaling pathway	28.26	15,00	CARD11, CCR7, CD226, G8P1, GCSAM, LCK, PRKCH, PRKD2, PTPN22, PVRIG, SH2D1A, SLA2, THY1, TRAT1, U8ASH3A
$CD8^+$ α/β T cell activation	35.71	10.00	CD274, CRTAM, EOMES, GPR18, LILR81, PTPN22, RUNX3, SAT81, SOCS1, TOX
$CD4^+$ $CD25^+$ α/β T cell cytokine production	34.78	8.00	CD55, GATA3, IL18R1, IL18, NLRP3, RSAD2, T8 × 21, TINAGL1
Regulation of T-helper type immune response	21.43	6.00	CCR2, HAVCR2, HLX, IL 18R1, IL18, IL1 RL1
NK T cell differentiation	50.00	6.00	ITK, PRDM1, SFTPA1, TOX, Z8T816, ZNF683
Lymphocyte chemotaxis	24.24	30.00	ADAM8, CCL11, CCL2, CCL20, CCL22, CCL3L 1, CCL4, CCL5, CCR2, CCR5, CCR7, CMKLR1, CXCL 10, CXCL 13, CXCL 14, CXCL2, CXCR3, CXCR6, EDN1, GCSAM, GPR75, GPR183, ITG87, KLRK1, PP8P, RIPOR2, S1PR1, STK39, ZAP70, XCR1
Regulation of IFN-y production	24.11	27.00	CCR2, CCR7, CD2, CD226, CD274, CD3E, CD96, CRTAM, E8I3, GATA3, HAVCR2, IL 10, IL 12R82, IL 18R1, IL18, IL1RL 1, INH8A, ISG15, KLRK1, LILR81, PDE48, PDE40, PTPN22, RASGRP1, TNF, ZC3H12A, ZFPM1
Chemokine-mediated signaling pathway	23.33	25.00	ADAM8, CCL 11, CCL2, CCL20, CCL22, CCL3L 1, CCL4, CCL5, CCR2, CCR5, CCR7, CMKLR1, CXCL 10, CXCL 13, CXCL 14, CXCL2, CXCR3, CXCR6, EDN1, GPR75, GPR183, KLRK1, PP8P, STK39, XCR1
Cytokine receptor activity	22.00	22.00	CCR2, CCR5, CCR7, CD4, CMKLR1, CRLF2, CXCR3, CXCR6, E8I3, GPR75, IL12R82, IL15RA, IL18R1, IL18RAP, IL1R2, IL1RAP, IL1RL1, IL21R, IL2RA, IL2R8, IL7R, XCR1
Natural killer cell mediated immunity	20.00	18.00	CD1A, CD1 D, CD226, CD96, CRTAM, GZM8, HAVCR2, KLRK1, F2RL1, ITGAM, LAG3, LILR81, RA827A, RASGRP1, SERPIN89, SH2D1A, SLAMF7, TINAGL 1
Regulation of IL-2 production	27.87	17.00	CARD11, CCR2, CD28, CD3E, CD4, GATA3, G8P1, HAVCR2, IL18, IRF4, LAG3, PDE48, PDE4O, PRKD2, SFTPD, T8 × 21, TNFAIP3, MEFV, TIGIT
Regulation of vitamin D biosynthetic process	44.00	12.00	ADAM8, CST7, IFNG, IL 10, IL 18, MMP8, NUPR1, SPHK1, SNAI1, TNF, TIMP1, TIMP3
Regulation of IL-12 production	20.00	12.00	ACP5, AGER, CCR7, CD40LG, CMKLR1, 1001, IFNG, IL 10, LILR81, LT8,
Negative regulation of IFN-I production	23.40	11.00	ACOD1, DHX58, HAVCR2, HERC5, IL 10, ISG15, LILR81, NLRC3, RNF125, TNFAIP3, U8E2L6
Negative regulation of IFN-γproduction	22.50	9.00	CD274, CD96, GATA3, HAVCR2, IL 10, IL 1RL 1, INH8A, LILR81, ZC3H12A
Positive regulation of leukocyte apoptotic process	23.53	8.00	ADAM8, CCL5, CD27, CD274, IDO1, IL10, NR4A3, PDCD1

(Continued on next page)

TABLE 2 (Continued)

GO term	% associated genes/term	No. of genes	Associated genes found
Regulation of lipopolysaccharide-mediated signaling pathway	20.00	8.00	ACOD1, CD180, CD55, F2RL 1, LTF, PTPN22, PRKCA, TNFAIP3
Regulation of IL-4 production	25.81	8.00	CD28, CD3E, CD40LG, GATA3, HAVCR2, IRF4, NLRP3, ZFPM1
Regulation of tolerance induction	35.00	7.00	CD274, CD3E, HAVCR2, IDO1, IL2RA, MARCHF7, PDCD1
Positive regulation of IL-5 production	46.15	6.00	CRLF2, GATA3, IL 1RAP, IL 1RL 1, NLRP3, PDE4O
Regulation of chronic inflammatory response	60.00	6.00	ADORA28, CCL5, IDO1, IL 10, TNF, TNFAIP3
Negative regulation of lymphocyte migration	28.67	4.00	CCL2, GCSAM, KLRK1, RIPOR2
Interleukin-1 receptor activity	57.14	4.00	IL18R1, IL 1 R2, IL 1 RAP, IL 1 RL 1
Negative regulation of IFN-α production	42.86	3.00	HAVCR2, IL 10, NLRC3
Positive regulation of apoptotic cell clearance	33.33	3.00	C3, C4A, CCL2
Epithelial cell morphogenesis	21.95	9.00	8CL 118, CCDC88C, CLDN3, COL 18A1, FAT1, FLN8, HEG1, HRH2, PECAM1
Other pathways			
Regulation of vascular endothelial growth factor production	21.21	7.00	ADORA28, C3, CCR2, HPSE, IL 18, RORA, SULF2
Regulation of extracellular matrix disassembly	21.05	4.00	CARMIL2, ETS1, FSCN1, PDPN
G protein-coupled purinergic nucleotide receptor activity	26.67	4.00	P2RY10, P2RY13, P2RY6, P2RY8
Inositol phosphate dephosphorylation	25.00	4.00	INPP1, INPP48, INPP58, SYNJ2

sue damage and hindering the inflammatory response observed mainly in Lena-infected piglets. A second possibility is that PRRSV might induce T-cell anergy if upregulation of inhibitory receptors is sustained over time and associated with a high level of viral antigen, as it has been described for other arterivirus, such as Equine arteritis virus (84). Although multiple elements are responsible for T-cell exhaustion (79), these findings, together with the well-known persistence of PRRSV in lymphoid organs (57), point out that PRRSV-1 could induce adaptive immune tolerance, making viral transmission in the farm easier.

Immune checkpoints were revealed as Hub genes conserved in both virulent and low-virulent PRRSV-1 infection. A Hub gene analysis was conducted by CytoHubba, since Hub genes set up more complex interactions compared with other genes in a PPI network and hence play a central role in the mechanisms of disease (85). Consequently, exploring Hub genes and their associated key pathways would be essential for a better understanding of PRRSV-1 infection at lung level. Eleven of 20 Hub genes were shared in both 3249 (Fig. 6) and Lena (Fig. 12) strains. Most of the Hub genes followed a similar kinetic for both strains, Lena and 3249, increasing their expression from 8 to 13 dpi. Nevertheless, several of them, SELL, *GZMB*, and *CCR7* (at 3 dpi), and *HAVCR2* (TIM-3), *TNFRSF9* (CD137), and *GPR18* (at 6 dpi) were promptly upregulated for the virulent Lena strain, probably associated with the marked clinical signs, the earlier and stronger peak of replication, and severe pneumonia. Remarkably, 13 of 20 Hub genes are considered as co-stimulatory immune checkpoints that are gaining a special interest nowadays, because of their role in cancer and chronic viral infections (86, 87). Mainly the Lena, but also the 3249 strain, induced an upregulation of co-stimulatory receptors such as *CD28*, *ICOS*, and several members of the TNF receptor family (*CD40LG* (CD154), *CD27*, *TNFRSF4* (OX40), *TNFRSF9* (CD137) and *TNFRSF18* (GITR)), which are considered as key players in $CD4^+$ and $CD8^+$ T-cell differentiation and expansion in acute and chronic viral infections (88–90). By contrast, co-inhibitory receptors, such as *CTLA4*, *CD274* (PD-L1), *PDCD1* (PD-1), *LAG3*, and *HAVCR2* (TIM-3), working together with IL-10, have been reported in acute viral infection, such as SARS-CoV-2 or influenza virus, playing a double role, one limiting inflammation induced tissue damage and ALI, as can particularly be the case for the virulent Lena strain, and another one, inducing a progressive dysfunction of T cells, impairing viral clearance and leading to chronic infection (33, 77, 79). A sustained upregulation of these Hub genes has been closely associated with $CD8^+$ and $CD4^+$ T-cells dysfunction during persistent viral infections together with high viral loads and antigen levels (33,

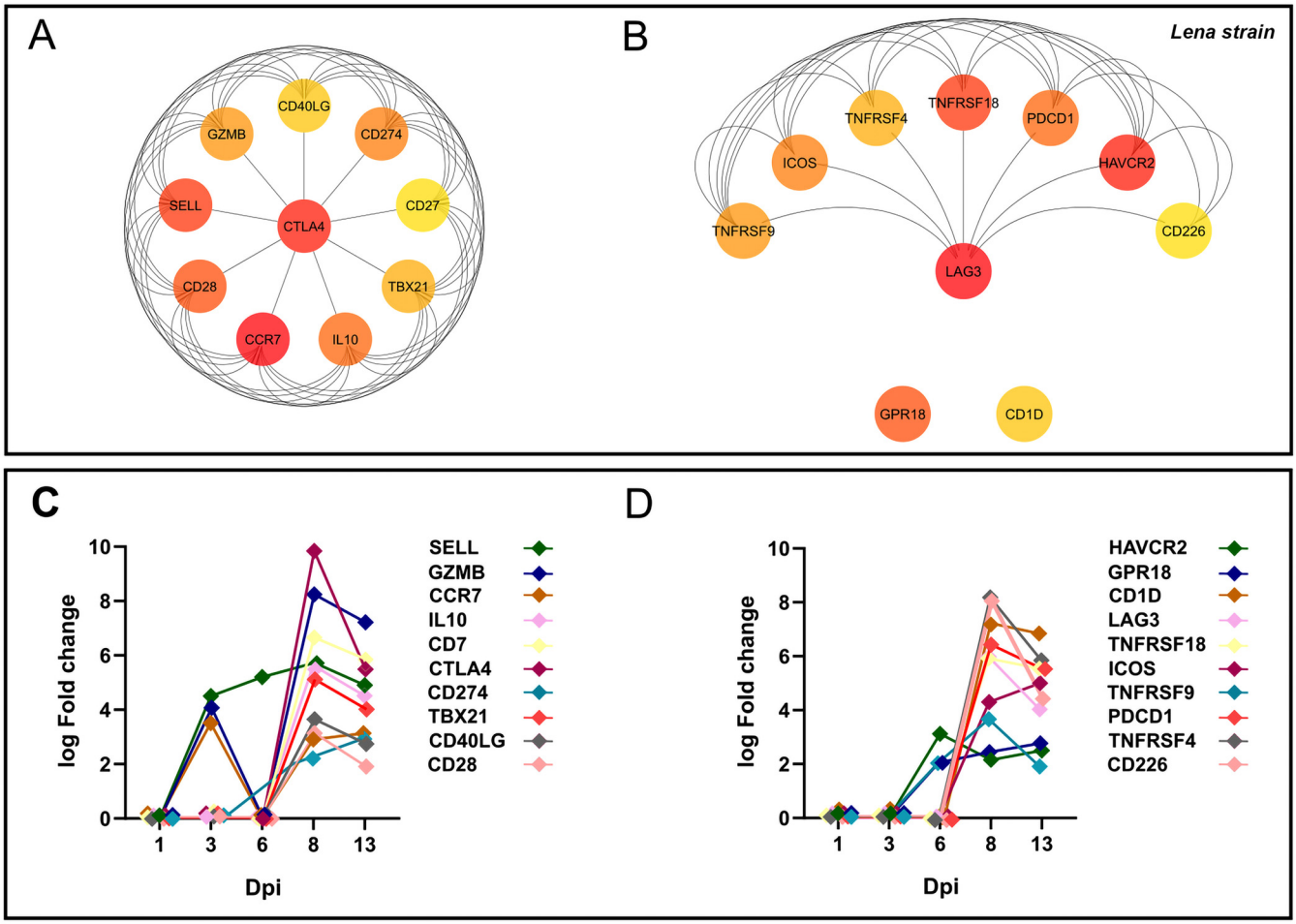

FIG 12 Hub genes network for virulent Lena strain. Hub genes for Lena strain were disclosed according to Maximal Clique Centrality (MCC) (A), and Density of Maximum Neighborhood Component (DMNC) (B) algorithms were identified from the whole PPI network. Kinetic of expression of Hub genes for Lena strain along the infection (C and D). The fold change for each Hub gene was illustrated as the median of the group at 1, 3, 6, 8, and 13 dpi.

79, 87). Subsequently, a MCODE analysis was conducted to evaluate the interaction of Hub genes with other DEGs, clustering most of them in cluster A in both Lena- and 3249-infected groups. Therefore, "regulation of lymphocyte apoptotic process," "T-cell selection," "positive regulation of IL-4 production," "T-cell co-stimulation," and "regulation of tolerance induction" seem to be significant pathways related to virulent Lena infection, whereas "positive regulation of leukocyte activation," "regulation of T-cell activation and differentiation," "lymphocyte migration," and "tolerance induction" would be the essential ones for the low-virulent 3249 strain. These results highlight that the mechanism of PRRSV infection with strains of different virulence could follow common pathways with a greater activation of pro- and anti-inflammatory response, and indeed, severe lung damage in Lena-infected piglets, probably associated with a superior replication rate (41).

CONCLUSION

The present study dissects the panoply of molecular mechanisms that govern the immunopathogenesis of PRRSV-1 infection with strains of different virulence at lung level, involving many conserved molecular pathways for virulent Lena and low-virulent 3249 strain. These included the activation of co-inhibitory and co-stimulatory immune checkpoints, revealed as Hub genes, in the pulmonary disease, which may have an impact on activation of $CD8^+$ and $CD4^+$ T cells and other T-cell related-pathways. Nevertheless, virulent Lena infection resulted in more pronounced and earlier

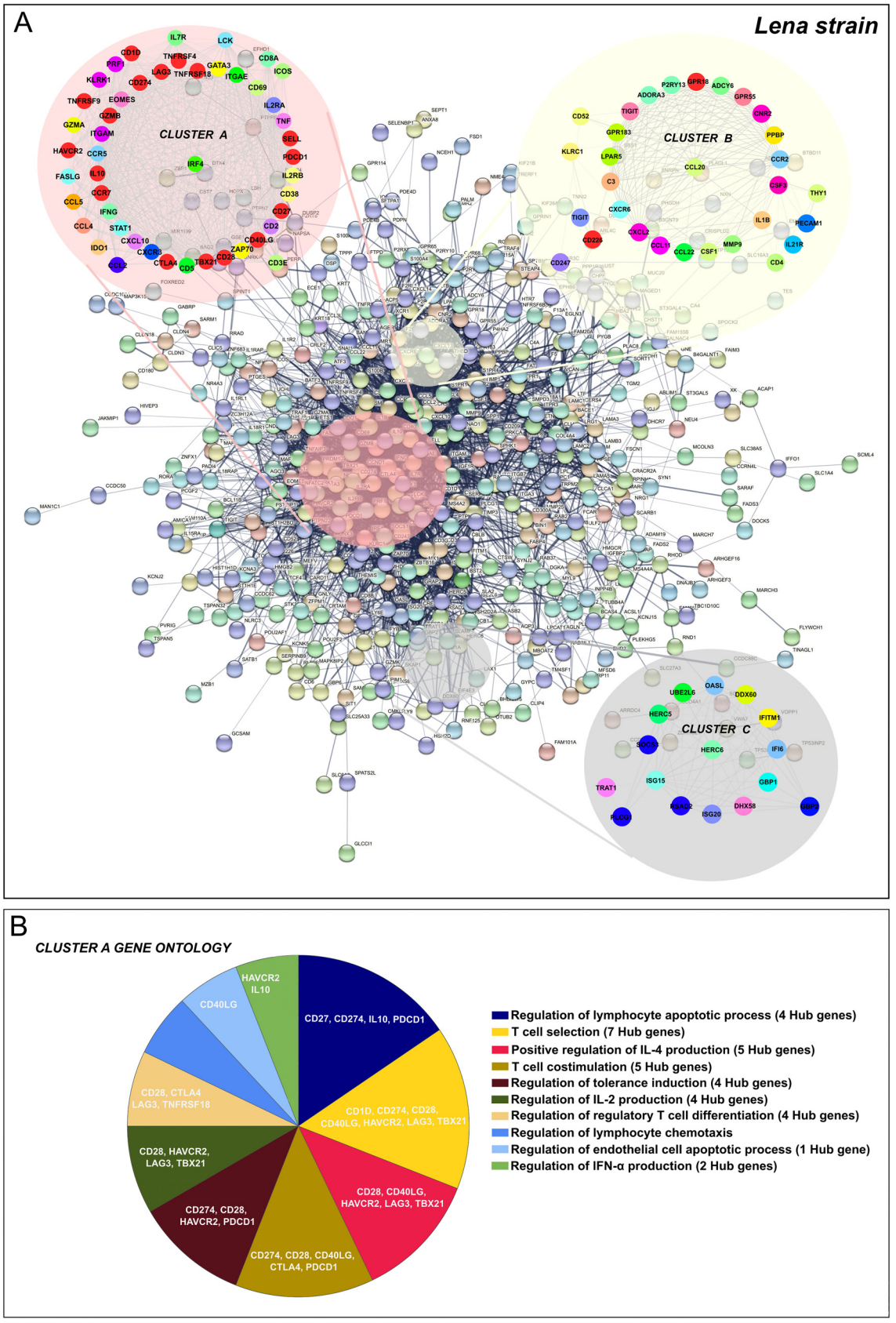

FIG 13 PPI network of 1,227 overlapped DEGs in response to Lena strain infection at 8–13 dpi (A). Network was constructed by STRING database and visualized by Cytoscape, underlining the significant clusters A, B, and C (k-core > 6), which were identified by

(Continued on next page)

TABLE 3 Gene Ontology (GO) analysis of Cluster A DEGs in response to Lena strain infection at 8–13 dpi

GO term	% associated genes/term	No. of genes	Associated genes found
Regulation of lymphocyte apoptotic process	12.50	13,00	CCL5, CCR7, CCR5, CXCR3, CD27, CD274, CD3E, IDO1, IL10, IL7R, IFNG, PDCD1, TNF
T cell selection	15.38	13,00	CCR7, CD1D, CD274, CD28, CD3E, CD40LG, IDO1, GATA3, HAVCR2, IRF4, LAG3, TBX21, ZAP70
Positive regulation of IL-4 production	25.00	10,00	CD28, CD3E, CD40LG, GATA3, HAVCR2, IRF4, LAG3, TBX21, STAT1, ZAP70
T cell co-stimulation	17.74	11,00	CCR7, CD274, CD28, CD3E, CD40LG, CD5, CTLA4, ICOS, KLRK1, LCK, PDCD1
Regulation of tolerance induction	26.32	9,00	CCL5, CD274, CD28, CD3E, HAVCR2, IDO1, IL2RA, PDCD1, ZAP70
Regulation of IL-2 production	11.29	7,00	CD28, CD3E, GATA3, HAVCR2, IRF4, LAG3, TBX21
Regulation of regulatory T cell differentiation	18.18	6,00	CD28, CTLA4, IFNG, IL2RA, LAG3, TNFRSF18
Regulation of lymphocyte chemotaxis	20.00	5,00	CCL2, CCL4, CCL5, CXCL10, KLRK1
Regulation of endothelial cell apoptotic process	10.20	5,00	CCL2, CD40LG, FASLG, GATA3, TNF
Regulation of IFN-α production	10.00	3,00	HACVR2, IL10, STAT1
IL-2 receptor activity	66.67	2,00	IL2RA, IL2RB

upregulation of these immune checkpoints together with the regulation of cytokine-signaling pathways, orchestrating an interplay among pro- and anti-inflammatory responses. These mechanisms try to restrict inflammation induced tissue damage and ALI, mostly in virulent Lena strain infection, but also may lead to a progressive dysfunction of T cells, impairing viral clearance and persistent infection, favoring secondary bacterial infections or viral rebound. This study highlights the pivotal role that immune checkpoints could play in responding to acute PRRSV-1 infection at the lung level, although further studies should be conducted to evaluate the functional role of immune checkpoints in chronic PRRSV infection and explore a possible T-cell exhaustion state.

MATERIALS AND METHODS

Porcine reproductive and respiratory syndrome virus strains. The low-virulent 3249 strain (subtype 1 PRRSV-1) was isolated from the serum of a piglet with pneumonia from a PRRSV-positive herd located in Spain in 2005 (91). The virulent Lena strain (subtype 3 PRRSV-1), considered as the prototype of PRRSV-1 virulent strains, was isolated from the lung of weak born piglets from a PRRSV outbreak characterized by high mortality rate, reproductive failure, and respiratory disorders in a Belarusian farm in 2007 (15). Both strains were propagated in porcine alveolar macrophages (PAMs), then the viral stocks were produced from the fourth passage of each strain, titrated by means of immunoperoxidase monolayer assay and expressed as tissue culture infectious doses 50 ($TCID_{50}$)/mL (Lena strain: $10^{5.66}$ $TCID_{50}$/mL; 3249 strain: $10^{5.79}$ $TCID_{50}$/mL).

Animals and experimental design. Animals used in this study belong to a large project carried out in order to investigate the pathogenesis of PRRSV-1 strains of different virulence (40). Briefly, 65 4-week-old piglets (Landrace $\times$ Large White crossbreed), obtained from a historically PRRSV-negative farm, were randomly assigned to three different groups and housed in separate pens in biosafety level III containment facilities (IRTA-CReSA, Cerdanyola del Vallès, Barcelona, Spain): 3249 group (n = 25), Lena group (n = 25), and control group (n = 15). At the beginning of the study, all piglets were ELISA and PCR-negative for porcine circovirus type 2 (PCV2), PRRSV, and *Mycoplasma hyopneumoniae* (92, 93).

After 1 week of acclimation, piglets were inoculated with the low-virulent 3249 strain or the virulent Lena strain (1 mL/nostril, 1×10^5 $TCID_{50}$/mL by intranasal inoculation with a mucosal atomizer; MAD Nasal Intranasal Mucosal Atomization Device, Teleflex, Alcalá de Henares, Madrid, Spain). The control group was mock-inoculated with PAMs supernatant diluted in RPMI 1640 culture medium (Thermo Fisher Scientific, Barcelona, Spain). Three piglets from each experimental group were euthanized at 1, 3, 6, 8, and 13 days postinoculation (dpi). All animal procedures were performed according to the guide-

FIG 13 Legend (Continued)
means of MCODE. The genes calculated by Maximal Clique Centrality (MCC) and Density of Maximum Neighborhood Component (DMNC) algorithms were selected as Hub genes (genes with the highest degree of connectivity) by CytoHubba plugin in Cytoscape. Most of the Hub genes (red color) were included in cluster A. GO enrichment analysis (BPs and ISPs categories) of DEGs included within cluster A (B). Overview pie chart showing the proportion of genes associated with the top functional groups, indicating the name of Hub genes in each term. Table 3 lists the top terms of GO (BPs and ISPs).

TABLE 4 Validation of RNA-seq gene expression patterns and Hub genes using RT-qPCR (log_2 fold change)[a]

		Fold increase (log_2)	
Gene	Quantification method	3249 strain	Lena strain
CD274 (PD-L1)	RNAseq	2.7	4.1
	qPCR	4.3	6.7
CTLA4	RNAseq	8.1	10.1
	qPCR	5.7	8.2
HACVR2 (TIM3)	RNAseq	-	2.2
	qPCR	-	5.1
LAG3	RNAseq	5.8	7.3
	qPCR	5.7	7.5
PDCD1 (PD-1)	RNAseq	5.3	6.4
	qPCR	5.7	7.5
IL10	RNAseq	-	5.6
	qPCR	-	7.3
TBX21 (T-bet)	RNAseq	3.6	5.1
	qPCR	4.1	7.1
CD28	RNAseq	2.4	3.2
	qPCR	3.9	6.5
TNFRSF9	RNAseq	3.9	5.9
	qPCR	3.9	6.9
GZMB	RNAseq	6.7	8.2
	qPCR	7.0	8.7
SELL	RNAseq	4.8	5.6
	qPCR	4.4	6.0
CCR7	RNAseq	-	2.8
	qPCR	-	3.1

[a]Dashes indicate not found as Hub gene for 3249 strain.

lines of the European Union (Directive 2010/63/EU) and approved by the IRTA Ethics Committee and by the Catalan Autonomous Government (Project 3647; FUE-2017-00533413).

Clinical signs, gross and histopathological lung lesion, and PRRSV lung viral load. Rectal temperature and clinical signs (liveliness, distress, and anorexia) were daily recorded from 2 days prior to inoculation until the end of the study. Hyperthermia was considered when rectal temperature was higher than 40.5°C. The score of clinical signs, ranging from 0 to 5, was recorded as previously described (41).

At necropsy, gross lung lesions were evaluated and recorded by the same pathologist as previously described by Halbur et al. (94). Parallel samples from cranial, middle, and caudal lobes of the right lung were collected and immediately frozen at −80°C for the quantification of lung viral load or fixed in 10% neutral buffered formalin (Fisher Scientific, Ltd., Loughborough, UK) for histopathological evaluation.

The histopathological findings were blindly evaluated and graded by two different pathologists. The severity of lung lesions for the interstitial pneumonia was scored as previously described (94), whereas the score for suppurative bronchopneumonia was previously described by Rodríguez-Gómez et al. (2019). Overall, the final score for each piglet was calculated as the sum of both the interstitial pneumonia and the bronchopneumonia scores.

A lung tissue homogenate was made previously to carry out RNA isolation and purification by using TRIzol LS Reagent (Thermo Fisher Scientific) followed by NucleoSpin RNA virus columns kit according to manufacturer's protocols (Macherey-Nagel, Düren, Germany). According to subgenomic copies of the virus, results for viral load were expressed by changes in quantification cycle (Cq), to not overestimate the number of PRRSV viral particles in the lung, as previously described (95). The ORF7 RT-PCR product from both 3249 and Lena strains was firstly precipitated in ethanol and purified using ExoSAP-ITTM (Thermo Fisher Scientific). The purified products were quantified using Nanodrop 2000 (Thermo Fisher Scientific). Serial 10-fold dilutions of 3249 or Lena ORF7 RT-PCR products (ranging from 10^8 to 10^2 genomic copies/mL) were used as standards to determine the limit of detection (1 copy/μL) and PCR efficiency (99%). Then, viral load for either Lena- or 3249-infected piglets was determined by RT-qPCR using VetMAX PRRSV EU/NA 2.0 kit (Thermo Fisher Scientific).

Flow cytometry (FCM) staining and analysis. BAL samples for FCM analysis and sequencing were collected at the time of necropsy from the left lung of each piglet (40). Freshly isolated cells from BAL were adjusted to 1.5×10^6 cells per sample in a final volume of 200 μL. Then, BAL cells were stained for CD163 (clone 2A10/11, IgG1, 10 μg/mL; Bio-Rad Laboratories, S.A., Alcobendas, Madrid, Spain). After washing, a second incubation step with a fluorochrome-labeled isotype-specific secondary antibody (Alexa Fluor 647 goat anti-mouse IgG1, 7 μg/mL; Invitrogen, Carlsbad, CA, USA) in combination with Live/Dead Fixable Aqua Dead Cell Stain (Invitrogen) was performed. Following surface labeling, cells were fixed and permeabilized with methanol overnight at −20°C (VWR International, Llinars del Vallès, Barcelona, Spain). FCM analysis was performed on a FACSCanto II (BD Biosciences, NJ, USA) recording

5×10^5 to 1×10^6 cells per sample. By making use of FlowJo software version 10 (FLOWJO LLC, Ashland, OR, USA), cells were gated according to light scatter properties (FSC-A versus SSC-A) and subjected to doublet (FSC-H versus FSC-W and SSC-H versus SSC-W) and dead cell discrimination and further analyzed for the expression of CD163.

BAL cells, RNA isolation, and sequencing. RNA seq analyses were performed on representative piglets (3 animals/group/time point) over time points ($n = 45$). These animals were selected according to their clinical signs, gross and microscopic lung lesion scores, as well as viral load. Total RNA was isolated from 1.5×10^6 cells per sample re-suspended with 1 ml of TRIzol reagent (Thermo Fisher Scientific), and then treated with Turbo DNA-free Kit (Thermo Fisher Scientific) to remove traces of contaminating genomic DNA (gDNA) following the manufacturer's guidelines. RNA integrity number (RIN) was assessed in the Bioanalyzer 2100 system (Agilent Technologies, CA, USA). All RNA samples used in the present study showed absence of gDNA and RIN values over 8.5.

Library preparation and sequencing were performed at the Functional Genomics Core of the Institute for Research in Biomedicine (IRB Barcelona, Spain). The cDNA libraries were prepared with 500 ng of total RNA for each individual sample using the Illumina TruSeq Stranded mRNA Sample Prep Kit (Illumina, Inc., San Diego, CA, USA). Libraries were quantified with Qubit dsDNA HS assay (Thermo Fisher Scientific) and quality was assessed by Agilent 2100 Bioanalyzer (Agilent Technologies). Subsequently, the indexed libraries were sequenced on a HiSeq2000 device (Illumina Inc.), and paired-end reads (2×75 base pair) were generated. The raw RNA-seq data set was deposited at NCBI Sequence Read Archive database with the accession number PRJNA704925.

RNA sequencing data processing, time-series, and DEG analysis. Bioinformatics analysis was carried out by the Andalusian Bioinformatics Platform of the University of Málaga. Raw data were firstly processed using the in-house customizable pre-processing pipeline SeqTrimNext (96). In this step, clean data (clean reads) were obtained by removing contaminants, sequencing adapters, PolyA/PolyT tails, and short ($<$ 17 nucleotide) and bad quality reads (Phred score $<$ 20); thus, all the downstream analyses were based on this high-quality clean data set. Then, clean reads were mapped to the reference porcine transcriptome (Sus_scrofa. Sscrofa11.1.cdna, with 46.076 unigenes) using Bowtie (v2.2.3) and Samtools (v1.9). The reads count of each transcript was extracted using the python script sam2counts.py (v0.91) (Buffalo, 2010).

Since our data were collected at different time points, a time-series analysis was conducted on clean data using MaSigPro R package (97) to identify clusters of genes with significant temporal expression changes related to 3249 and Lena strain infection over time. Afterwards, DEgenes Hunter R pipeline and DeSeq2 R package (98) were used to identify differentially expressed genes (DEGs) between both infected groups and control group at each time point (1, 3, 6, 8, and 13 dpi). The *P values* were adjusted using Benjamini and Hochberg's correction for controlling the false discovery rate (FDR). Genes with an FDR $<$ 0.05 and an absolute $\log_2$ fold change (log2FC) $\geq$ 1 were assigned as DEGs. The DEGs of Lena- and 3249-infected groups' data set for each time point were visualized as a volcano plot by using GraphPad Prism (GraphPad Prism software v8.0), underlining the top 5 DEGs with a higher log2FC. Overlapped DEGs at 1, 3, 6, 8, and 13 dpi from Lena- or 3249-infected animals were identified and presented as a Venn diagram using an online tool (http://bioinformatics.psb.ugent.be/webtools/Venn/).

Gene ontology (GO) and pathway enrichment analysis. In order to explore GO of DEGs (http://geneontology.org), functional enrichment analyses were conducted using ClueGO (v2.3.3) and CluePedia (v1.3.3), plugins for Cytoscape (v3.8, http://cytoscape.org/) describing biological processes (BPs) and immune system processes (ISPs) GO categories. ClueGO determines the distribution of the DEGs for various GO terms and pathways, generating a functionally grouped GO annotation network (99, 100). The *P* value was calculated using right-sided hypergeometric tests and the Benjamini and Hochberg's correction for multiple testing (FDR $<$ 0.05). This FDR threshold, together with a high kappa value (0.4), enabled us to precisely select significantly enriched and highly connected GO terms. The most significant term defines the name of the group. In order to avoid over-interpretation of data, a minimum of 3 genes were considered to evaluate the relevance of selected pathways.

Construction of protein-protein interaction (PPI) network and screening of Hub genes. The Search Tool for the Retrieval of Interacting Genes (STRING) database was applied to predict PPI and construct a PPI network of selected DEGs (101). Using the STRING database, DEGs with a score $\geq$ 0.4 were chosen to build a network model visualized by Cytoscape (102). Molecular complex detection (MCODE) is a Cytoscape plugin used to identify the finest PPI sub-network modules (102). The Hub genes are defined as genes with the highest degree of connectivity in the key module. Since the biological networks usually are heterogeneous, it seems to be reasonable to use more than one method for identifying Hub nodes (103); thus, Maximal Clique Centrality (MCC) and Density of Maximum Neighborhood Component (DMNC) algorithms were calculated for each node by CytoHubba plugin in Cytoscape (103). The genes with the top 10 MCC and DMNC values were considered as Hub genes.

Real-time quantitative reverse transcriptase PCR (RT-qPCR). To verify the major results drawn from RNA-seq and Hub genes analysis, the expression levels of a panel of 12 identified Hub genes were performed by RT-qPCR. cDNA was synthesized by reverse transcription using iScript cDNA Synthesis Kit (Bio-Rad) from 1 μg of the original RNA sample used for the RNA-seq according to manufacturer's guidelines. Subsequently, amplifications were run in triplicate using iTaq Universal SYBR Green Supermix (Bio-Rad) on the MyiQ2 Two-Color Real-Time PCR Detection System (Bio-Rad). For each reaction well, 50 ng of cDNA from each animal and 0.5 μM each primer were used. *GAPDH* was chosen as reference gene, and the relative expression level of each Hub gene was calculated by the $2^{-\Delta\Delta Ct}$ method (104). The primers set used for RT-qPCR are listed in Table 5.

TABLE 5 Primer sequences of Hub genes used to validate RNA-seq analysis

Gene	Sequences	Reference
GAPDH	F 5′-ACATGGCCTCCAAGGAGTAAGA-3″	105
	R 5′-GATCGAGTTGGGGCTGTGACT-3″	
CD274 (PD-L1)	F 5′-GTGGAAAAATGTGGCAGCCG-3″	Self-designed
	R 5′-TGCTTAGCCCTGACGAACTC-3″	
CTLA4	F 5′-TCTTCATCCCTGTCTTCTCCAAA-3″	106
	R 5′-GCAGACCCATACTCACACACAAA-3″	
HACVR2 (TIM3)	F 5′-TTCGACGGGAGCAGTAAAGC-3″	Self-designed
	R 5′-AGGGCAGGACACAGTCAAAG-3″	
LAG3	F 5-CTCCTCCTGCTCCTTTTGGTT-3″	106
	R 5′-CAGCTCCCCAGTCTTGCTCT-3″	
PDCD1 (PD-1)	F 5′- AGCCCAAGCACTTCATCCTC-3″	Self-designed
	R 5′- TGTGGAAGTCTCGTCCGTTG-3″	
IL10	F 5′- TGAGAACAGCTGCATCCACTTC -3″	107
	R 5′- TCTGGTCCTTCGTTTGAAAGAAA -3″	
TBX21 (T-bet)	F 5′- TGCAGTCCCTCCATAAGTACCA -3″	108
	R 5′- GCCTCTGGCTCACCATCATT -3″	
CD28	F 5′-CCCCTCAATTCAAGTAACAGGAAAC-3″	Self-designed
	R 5′- ATGCCCGGAACTCCTTTGAG-3″	
TNFRSF9	F 5′-TTGCCAGCAAGGTCAAGAGT-3″	Self-designed
	R 5′- AGCCAAAGAACAGTCCGTCC-3″	
GZMB	F 5′-GCCCCTACATGGCGTATCTTC-3″	Self-designed
	R 5′- ACGTTGATTGAGCTTCCCCA-3″	
SELL	F 5′-CCTAGTCCGATATGTCAAAAACTGG-3′	Self-designed
	R 5′- TCATCCATGCTTCTCTGAGACTT-3″	
CCR7	F 5′-TTGTCATTTTCCAGGTGTGCC-3″	Self-designed
	R 5′- GGAGTACATGACCGGGAGGA-3″	

Data availability. The raw RNA-seq data set was deposited at NCBI Sequence Read Archive database with the accession number PRJNA704925.

ACKNOWLEDGMENTS

The authors thank Alberto Alcántara and Gema Muñoz for their technical assistance. J. Gómez-Laguna is supported by a "Ramón y Cajal" contract of the Spanish Ministry of Economy and Competitiveness (RYC-2014-16735). J. M. Sánchez-Carvajal was supported by a postdoctoral research contract from the University of Córdoba (Plan propio 2020). This work was supported by the Spanish Ministry of Economy and Competitiveness (#AGL2016-76111-R and PID2019-109718GB-I00).

We declare that we have no conflicts of interest.

REFERENCES

1. Nathues H, Alarcon P, Rushton J, Jolie R, Fiebig K, Jimenez M, Geurts V, Nathues C. 2017. Cost of porcine reproductive and respiratory syndrome virus at individual farm level—An economic disease model. Prev Vet Med 142:16–29. https://doi.org/10.1016/j.prevetmed.2017.04.006.
2. Holtkamp DJ, Kliebenstein JB, Neumann EJ, Zimmerman JJ, Rotto HF, Yoder TK, Wang C, Yeske PE, Mowrer CL, Haley CA. 2013. Assessment of the economic impact of porcine reproductive and respiratory syndrome virus on United States pork producers. J Swine Heal Prod 21:72–84.
3. Meulenberg JJM, Hulst MM, De Meijer EJ, Moonen PLJM, Den Besten A, De Kluyver EP, Wensvoort G, Moormann RJM. 1993. Lelystad virus, the causative agent of porcine epidemic abortion and respiratory syndrome (PEARS), is related to LDV and EAV. Virology 192:62–72. https://doi.org/10.1006/viro.1993.1008.
4. Wensvoort G, Terpstra C, Pol JM, ter Laak EA, Bloemraad M, de Kluyver EP, Kragten C, van Buiten L, den Besten A, Wagenaar F. 1991. Mystery swine disease in The Netherlands: the isolation of Lelystad virus. Vet Q 13:121–130. https://doi.org/10.1080/01652176.1991.9694296.
5. Brinton MA, Gulyaeva A, Balasuriya UBR, Dunowska M, Faaberg KS, Goldberg T, Leung FC, Nauwynck HJ, Snijder EJ, Stadejek T, Gorbalenya AE. 2018. Proposal 2017.012S.A.v1. Expansion of the rank structure of the family *Arteriviridae* and renaming its taxa. https://talk.ictvonline.org/ICTV/proposals/2017.001S.012-017S.R.Nidovirales.zip. Accessed 15 October 2021.
6. Balka G, Podgórska K, Brar MS, Bálint Á, Cadar D, Celer V, Dénes L, Dirbakova Z, Jedryczko A, Márton L, Novosel D, Petrović T, Sirakov I, Szalay D, Toplak I, Leung FCC, Stadejek T. 2018. Genetic diversity of PRRSV 1 in Central Eastern Europe in 1994–2014: origin and evolution of the virus in the region. Sci Rep 8:7811. https://doi.org/10.1038/s41598-018-26036-w.
7. Stadejek T, Stankevicius A, Murtaugh MP, Oleksiewicz MB. 2013. Molecular evolution of PRRSV in Europe: current state of play. Vet Microbiol 165:21–28. https://doi.org/10.1016/j.vetmic.2013.02.029.
8. Shi M, Lam TTY, Hon CC, Hui RKH, Faaberg KS, Wennblom T, Murtaugh MP, Stadejek T, Leung FCC. 2010. Molecular epidemiology of PRRSV: a phylogenetic perspective. Virus Res 154:7–17. https://doi.org/10.1016/j.virusres.2010.08.014.
9. Ogno G, Rodríguez-Gómez IM, Canelli E, Ruedas-Torres I, Álvarez B, Domínguez J, Borghetti P, Martelli P, Gómez-Laguna J. 2019. Impact of PRRSV strains of different in vivo virulence on the macrophage population of the thymus. Vet Microbiol 232:137–145. https://doi.org/10.1016/j.vetmic.2019.04.016.
10. Canelli E, Catella A, Borghetti P, Ferrari L, Ogno G, De Angelis E, Corradi A, Passeri B, Bertani V, Sandri G, Bonilauri P, Leung FC, Guazzetti S,

Martelli P. 2017. Phenotypic characterization of a highly pathogenic Italian porcine reproductive and respiratory syndrome virus (PRRSV) type 1 subtype 1 isolate in experimentally infected pigs. Vet Microbiol 210:124–133. https://doi.org/10.1016/j.vetmic.2017.09.002.
11. Sinn LJ, Klingler E, Lamp B, Brunthaler R, Weissenböck H, Rümenapf T, Ladinig A. 2016. Emergence of a virulent porcine reproductive and respiratory syndrome virus (PRRSV) 1 strain in Lower Austria. Porc Heal Manag 2:28. https://doi.org/10.1186/s40813-016-0044-z.
12. Morgan SB, Frossard JP, Pallares FJ, Gough J, Stadejek T, Graham SP, Steinbach F, Drew TW, Salguero FJ. 2016. Pathology and virus distribution in the lung and lymphoid tissues of pigs experimentally inoculated with three distinct type 1 PRRS virus isolates of varying pathogenicity. Transbound Emerg Dis 63:285–295. https://doi.org/10.1111/tbed.12272.
13. Morgan SB, Graham SP, Salguero FJ, Sánchez Cordón PJ, Mokhtar H, Rebel JMJ, Weesendorp E, Bodman-Smith KB, Steinbach F, Frossard JP. 2013. Increased pathogenicity of European porcine reproductive and respiratory syndrome virus is associated with enhanced adaptive responses and viral clearance. Vet Microbiol 163:13–22. https://doi.org/10.1016/j.vetmic.2012.11.024.
14. Weesendorp E, Morgan S, Stockhofe-Zurwieden N, De Graaf DJP, Graham SP, Rebel JMJ. 2013. Comparative analysis of immune responses following experimental infection of pigs with European porcine reproductive and respiratory syndrome virus strains of differing virulence. Vet Microbiol 163:1–12. https://doi.org/10.1016/j.vetmic.2012.09.013.
15. Karniychuk UU, Geldhof M, Vanhee M, Van Doorsselaere J, Saveleva TA, Nauwynck HJ. 2010. Pathogenesis and antigenic characterization of a new East European subtype 3 porcine reproductive and respiratory syndrome virus isolate. BMC Vet Res 6:30. https://doi.org/10.1186/1746-6148-6-30.
16. Huang C, Zhang Q, Feng W. 2015. Regulation and evasion of antiviral immune responses by porcine reproductive and respiratory syndrome virus. Virus Res 202:101–111. https://doi.org/10.1016/j.virusres.2014.12.014.
17. Loving CL, Osorio FA, Murtaugh MP, Zuckermann FA. 2015. Innate and adaptive immunity against porcine reproductive and respiratory syndrome virus. Vet Immunol Immunopathol 167:1–14. https://doi.org/10.1016/j.vetimm.2015.07.003.
18. Butler JE, Lager KM, Golde W, Faaberg KS, Sinkora M, Loving C, Zhang YI. 2014. Porcine reproductive and respiratory syndrome (PRRS): an immune dysregulatory pandemic. Immunol Res 59:81–108. https://doi.org/10.1007/s12026-014-8549-5.
19. Han J, Zhou L, Ge X, Guo X, Yang H. 2017. Pathogenesis and control of the Chinese highly pathogenic porcine reproductive and respiratory syndrome virus. Vet Microbiol 209:30–47. https://doi.org/10.1016/j.vetmic.2017.02.020.
20. Lunney JK, Fang Y, Ladinig A, Chen N, Li Y, Rowland B, Renukaradhya GJ. 2016. Porcine reproductive and respiratory syndrome virus (PRRSV): pathogenesis and interaction with the immune system. Annu Rev Anim Biosci 4:129–154. https://doi.org/10.1146/annurev-animal-022114-111025.
21. Mair KH, Sedlak C, Käser T, Pasternak A, Levast B, Gerner W, Saalmüller A, Summerfield A, Gerdts V, Wilson HL, Meurens F. 2014. The porcine innate immune system: An update. Dev Comp Immunol 45:321–343. https://doi.org/10.1016/j.dci.2014.03.022.
22. Mateu E, Diaz I. 2008. The challenge of PRRS immunology. Vet J 177:345–351. https://doi.org/10.1016/j.tvjl.2007.05.022.
23. Gómez-Laguna J, Salguero FJ, Pallarés FJ, Carrasco L. 2013. Immunopathogenesis of porcine reproductive and respiratory syndrome in the respiratory tract of pigs. Vet J 195:148–155. https://doi.org/10.1016/j.tvjl.2012.11.012.
24. Lim B, Kim S, Lim KS, Jeong CG, Kim SC, Lee SM, Park CK, Te Pas MFW, Gho H, Kim TH, Lee KT, Kim W, Il, Kim JM. 2020. Integrated time-serial transcriptome networks reveal common innate and tissue-specific adaptive immune responses to PRRSV infection. Vet Res 51:128. https://doi.org/10.1186/s13567-020-00850-5.
25. Xiao S, Mo D, Wang Q, Jia J, Qin L, Yu X, Niu Y, Zhao X, Liu X, Chen Y. 2010. Aberrant host immune response induced by highly virulent PRRSV identified by digital gene expression tag profiling. BMC Genomics 11:544. https://doi.org/10.1186/1471-2164-11-544.
26. Xiao S, Jia J, Mo D, Wang Q, Qin L, He Z, Zhao X, Huang Y, Li A, Yu J, Niu Y, Liu X, Chen Y. 2010. Understanding PRRSV infection in porcine lung based on genome-wide transcriptome response identified by deep sequencing. PLoS One 5:e11377. https://doi.org/10.1371/journal.pone.0011377.
27. Wilkinson JM, Ladinig A, Bao H, Kommadath A, Stothard P, Lunney JK, Harding JCS, Plastow GS. 2016. Differences in whole blood gene expression associated with infection time-course and extent of fetal mortality in a reproductive model of type 2 porcine reproductive and respiratory syndrome virus (PRRSV) infection. PLoS One 11:e0153615. https://doi.org/10.1371/journal.pone.0153615.
28. Schroyen M, Eisley C, Koltes JE, Fritz-Waters E, Choi I, Plastow GS, Guan L, Stothard P, Bao H, Kommadath A, Reecy JM, Lunney JK, Rowland RRR, Dekkers JCM, Tuggle CK. 2016. Bioinformatic analyses in early host response to porcine reproductive and respiratory syndrome virus (PRRSV) reveals pathway differences between pigs with alternate genotypes for a major host response QTL. BMC Genomics 17:196. https://doi.org/10.1186/s12864-016-2547-z.
29. Badaoui B, Rutigliano T, Anselmo A, Vanhee M, Nauwynck H, Giuffra E, Botti S. 2014. RNA-sequence analysis of primary alveolar macrophages after in vitro infection with porcine reproductive and respiratory syndrome virus strains of differing virulence. PLoS One 9:e91918. https://doi.org/10.1371/journal.pone.0091918.
30. Chen Z, Liu S, Zhang S, Zhang Y, Yu J, Sun W, Chen L, Du Y, Wang J, Li Y, Wu J. 2018. Porcine reproductive and respiratory syndrome virus strains with higher virulence cause marked protein profile changes in MARC-145 cells. Sci Rep 8:15000. https://doi.org/10.1038/s41598-018-32984-0.
31. Miller LC, Fleming D, Arbogast A, Bayles DO, Guo B, Lager KM, Henningson JN, Schlink SN, Yang HC, Faaberg KS, Kehrli ME. 2012. Analysis of the swine tracheobronchial lymph node transcriptomic response to infection with a Chinese highly pathogenic strain of porcine reproductive and respiratory syndrome virus. BMC Vet Res 8:208. https://doi.org/10.1186/1746-6148-8-208.
32. Dong Q, Lunney J, Fritz-Waters E, Nguyen Y, Rowland B, Hess AS, Reecy JM, Dekkers JCM. 2017. The effect of PRRS viral level and isolate on tonsil gene expression. Iowa State University Animal Industry Report 14(1). https://doi.org/10.31274/ans_air-180814-299.
33. Cai H, Liu G, Zhong J, Zheng K, Xiao H, Li C, Song X, Li Y, Xu C, Wu H, He Z, Zhu Q. 2020. Immune checkpoints in viral infections. Viruses 12:1051. https://doi.org/10.3390/v12091051.
34. Chen S, Bonifati S, Qin Z, Gelais CS, Kodigepalli KM, Barrett BS, Kim SH, Antonucci JM, Ladner KJ, Buzovetsky O, Knecht KM, Xiong Y, Yount JS, Guttridge DC, Santiago ML, Wu L. 2018. SAMHD1 suppresses innate immune responses to viral infections and inflammatory stimuli by inhibiting the NF-κB and interferon pathways. Proc Natl Acad Sci U S A 115:E3798–E3807. https://doi.org/10.1073/pnas.1801213115.
35. Anandasabapathy N, Ford GS, Bloom D, Holness C, Paragas V, Seroogy C, Skrenta H, Hollenhorst M, Fathman CG, Soares L. 2003. GRAIL: an E3 ubiquitin ligase that inhibits cytokine gene transcription is expressed in anergic CD4+ T cells. Immunity 18:535–547. https://doi.org/10.1016/s1074-7613(03)00084-0.
36. Martinet L, Smyth MJ. 2015. Balancing natural killer cell activation through paired receptors. Nat Rev Immunol 15:243–254. https://doi.org/10.1038/nri3799.
37. Thio CL, Mosbruger TL, Kaslow RA, Karp CL, Strathdee SA, Vlahov D, O'Brien SJ, Astemborski J, Thomas DL. 2004. Cytotoxic T-lymphocyte antigen 4 gene and recovery from hepatitis B virus infection. J Virol 78:11258–11262. https://doi.org/10.1128/JVI.78.20.11258-11262.2004.
38. Harjunpää H, Guillerey C. 2020. TIGIT as an emerging immune checkpoint. Clin Exp Immunol 200:108–119. https://doi.org/10.1111/cei.13407.
39. Renson P, Rose N, Le Dimna M, Mahé S, Keranflec'h A, Paboeuf F, Belloc C, Le Potier M-F, Bourry O. 2017. Dynamic changes in bronchoalveolar macrophages and cytokines during infection of pigs with a highly or low pathogenic genotype 1 PRRSV strain. Vet Res 48:15. https://doi.org/10.1186/s13567-017-0420-y.
40. Rodríguez-Gómez IMIM, Sánchez-Carvajal JM, Pallarés FJFJ, Mateu E, Carrasco L, Gómez-Laguna J. 2019. Virulent Lena strain induced an earlier and stronger downregulation of CD163 in bronchoalveolar lavage cells. Vet Microbiol 235:101–109. https://doi.org/10.1016/j.vetmic.2019.06.011.
41. Sánchez-Carvajal JM, Rodríguez-Gómez IM, Ruedas-Torres I, Larenas-Muñoz F, Díaz I, Revilla C, Mateu E, Domínguez J, Martín-Valls G, Barranco I, Pallarés FJ, Carrasco L, Gómez-Laguna J. 2020. Activation of pro- and anti-inflammatory responses in lung tissue injury during the acute phase of PRRSV-1 infection with the virulent strain Lena. Vet Microbiol 246:108744. https://doi.org/10.1016/j.vetmic.2020.108744.
42. Sánchez-Carvajal JM, Ruedas-Torres I, Carrasco L, Pallarés FJ, Mateu E, Rodríguez-Gómez IM, Gómez-Laguna J. 2021. Activation of regulated cell death in the lung of piglets infected with virulent PRRSV-1 Lena

strain occurs earlier and mediated by cleaved Caspase-8. Vet Res 52:12. https://doi.org/10.1186/s13567-020-00882-x.
43. Ketter E, Randall G. 2019. Virus impact on lipids and membranes. Annu Rev Virol 6:319–340. https://doi.org/10.1146/annurev-virology-092818-015748.
44. Schoggins JW, Rice CM. 2011. Interferon-stimulated genes and their antiviral effector functions. Curr Opin Virol 1:519–525. https://doi.org/10.1016/j.coviro.2011.10.008.
45. Schoggins JW. 2019. Interferon-stimulated genes: what do they all do? Annu Rev Virol 6:567–584. https://doi.org/10.1146/annurev-virology-092818-015756.
46. Fleming DS, Miller LC, Tian Y, Li Y, Ma W, Sang Y. 2020. Impact of porcine arterivirus, influenza B, and their coinfection on antiviral response in the porcine lung. Pathogens 9:934–919. https://doi.org/10.3390/pathogens9110934.
47. Zhou P, Zhai S, Zhou X, Lin P, Jiang T, Hu X, Jiang Y, Wu B, Zhang Q, Xu X, Ping Li J, Liu B. 2011. Molecular characterization of transcriptome-wide interactions between highly pathogenic porcine reproductive and respiratory syndrome virus and porcine alveolar macrophages in vivo. Int J Biol Sci 7:947–959. https://doi.org/10.7150/ijbs.7.947.
48. Lee AJ, Ashkar AA. 2018. The dual nature of type I and type II interferons. Front Immunol 9:2061. https://doi.org/10.3389/fimmu.2018.02061.
49. Liu K, Li Y, Zhou B, Wang F, Huan B, Shao D, Wei J, Qiu Y, Li B, Qian Y, Jung YS, Miao D, Tong G, Ma Z. 2017. A conjugate protein containing HIV TAT, ISG20, and a PRRSV polymerase binding inhibits PRRSV replication and may be a novel therapeutic platform. Res Vet Sci 113:13–20. https://doi.org/10.1016/j.rvsc.2017.08.008.
50. Fang J, Wang H, Bai J, Zhang Q, Li Y, Liu F, Jiang P. 2016. Monkey viperin restricts porcine reproductive and respiratory syndrome virus replication. PLoS One 11:e0156513. https://doi.org/10.1371/journal.pone.0156513.
51. Li Y, Liang S, Liu H, Sun Y, Kang L, Jiang Y. 2015. Identification of a short interspersed repetitive element insertion polymorphism in the porcine MX1 promoter associated with resistance to porcine reproductive and respiratory syndrome virus infection. Anim Genet 46:437–440. https://doi.org/10.1111/age.12316.
52. Huang C, Du Y, Yu Z, Zhang Q, Liu Y, Tang J, Shi J, Feng WH. 2016. Highly pathogenic porcine reproductive and respiratory syndrome virus Nsp4 cleaves VISA to impair antiviral responses mediated by RIG-I-like receptors. Sci Rep 6:28497–28413. https://doi.org/10.1038/srep28497.
53. Sun Y, Han M, Kim C, Calvert JG, Yoo D. 2012. Interplay between interferon-mediated innate immunity and porcine reproductive and respiratory syndrome virus. Viruses 4:424–446. https://doi.org/10.3390/v4040424.
54. Han M, Yoo D. 2014. Modulation of innate immune signaling by nonstructural protein 1 (nsp1) in the family Arteriviridae. Virus Res 194:100–109. https://doi.org/10.1016/j.virusres.2014.09.007.
55. Yoo D, Song C, Sun Y, Du Y, Kim O, Liu HC. 2010. Modulation of host cell responses and evasion strategies for porcine reproductive and respiratory syndrome virus. Virus Res 154:48–60. https://doi.org/10.1016/j.virusres.2010.07.019.
56. Huang C, Zhang Q, Guo X.-k, Yu Z.-b, Xu A-T, Tang J, Feng W-h. 2014. Porcine reproductive and respiratory syndrome virus nonstructural protein 4 antagonizes beta interferon expression by targeting the NF- B essential modulator. J Virol 88:10934–10945. https://doi.org/10.1128/JVI.01396-14.
57. Wills RW, Doster AR, Galeota JA, Sur JH, Osorio FA. 2003. Duration of infection and proportion of pigs persistently infected with porcine reproductive and respiratory syndrome virus. J Clin Microbiol 41:58–62. https://doi.org/10.1128/JCM.41.1.58-62.2003.
58. Amarilla SP, Gómez-Laguna J, Carrasco L, Rodríguez-Gómez IM, Caridad y Ocerín JM, Morgan SB, Graham SP, Frossard JP, Drew TW, Salguero FJ. 2015. A comparative study of the local cytokine response in the lungs of pigs experimentally infected with different PRRSV-1 strains: upregulation of IL-1α in highly pathogenic strain induced lesions. Vet Immunol Immunopathol 164:137–147. https://doi.org/10.1016/j.vetimm.2015.02.003.
59. Weesendorp E, Rebel JMJ, Popma-De Graaf DJ, Fijten HPD, Stockhofe-Zurwieden N. 2014. Lung pathogenicity of European genotype 3 strain porcine reproductive and respiratory syndrome virus (PRRSV) differs from that of subtype 1 strains. Vet Microbiol 174:127–138. https://doi.org/10.1016/j.vetmic.2014.09.010.
60. Haine V, Fischer-Smith T, Rappaport J. 2006. Macrophage colony-stimulating factor in the pathogenesis of HIV infection: potential target for therapeutic intervention. J Neuroimmune Pharmacol 1:32–40. https://doi.org/10.1007/s11481-005-9003-1.
61. Vassiliou AG, Kotanidou A, Dimopoulou I, Orfanos SE. 2020. Endothelial damage in acute respiratory distress syndrome. Int J Mol Sci 21:8793. https://doi.org/10.3390/ijms21228793.
62. Camp JV, Jonsson CB. 2017. A role for neutrophils in viral respiratory disease. Front Immunol 8:550. https://doi.org/10.3389/fimmu.2017.00550.
63. Kallal LE, Schaller MA, Lindell DM, Lira SA, Lukacs NW. 2010. CCL20/CCR6 blockade enhances immunity to RSV by impairing recruitment of DC. Eur J Immunol 40:1042–1052. https://doi.org/10.1002/eji.200939778.
64. Mahalingam S, Friedland JS, Heise MT, Rulli NE, Meanger J, Lidbury BA. 2003. Chemokines and viruses: Friends or foes? Trends Microbiol 11:383–391. https://doi.org/10.1016/s0966-842x(03)00157-4.
65. Blumer T, Coto-Llerena M, Duong FHT, Heim MH. 2017. SOCS1 is an inducible negative regulator of interferon λ (IFN-λ)-induced gene expression in vivo. J Biol Chem 292:17928–17938. https://doi.org/10.1074/jbc.M117.788877.
66. Calzada-Nova G, Schnitzlein WM, Husmann RJ, Zuckermann FA. 2011. North American porcine reproductive and respiratory syndrome viruses inhibit type I interferon production by plasmacytoid dendritic cells. J Virol 85:2703–2713. https://doi.org/10.1128/JVI.01616-10.
67. Van Gucht S, Van Reeth K, Pensaert M. 2003. Interaction between porcine reproductive-respiratory syndrome virus and bacterial endotoxin in the lungs of pigs: potentiation of cytokine production and respiratory disease. J Clin Microbiol 41:960–966. https://doi.org/10.1128/JCM.41.3.960-966.2003.
68. Van Reeth K, Nauwynck H. 2000. Proinflammatory cytokines and viral respiratory disease in pigs. Vet Res 31:187–213. https://doi.org/10.1051/vetres:2000113.
69. Gómez-Laguna J, Salguero FJ, Barranco I, Pallarés FJ, Rodríguez-Gómez IM, Bernabé A, Carrasco L. 2010. Cytokine expression by macrophages in the lung of pigs infected with the porcine reproductive and respiratory syndrome virus. J Comp Pathol 142:51–60. https://doi.org/10.1016/j.jcpa.2009.07.004.
70. Silva-Campa E, Cordoba L, Fraile L, Flores-Mendoza L, Montoya M, Hernández J. 2010. European genotype of porcine reproductive and respiratory syndrome (PRRSV) infects monocyte-derived dendritic cells but does not induce Treg cells. Virology 396:264–271. https://doi.org/10.1016/j.virol.2009.10.024.
71. Rodríguez-Gómez IM, Käser T, Gómez-Laguna J, Lamp B, Sinn L, Rümenapf T, Carrasco L, Saalmüller A, Gerner W. 2015. PRRSV-infected monocyte-derived dendritic cells express high levels of SLA-DR and CD80/86 but do not stimulate PRRSV-naïve regulatory T cells to proliferate. Vet Res 46:54. https://doi.org/10.1186/s13567-015-0186-z.
72. Silva-Campa E, Flores-Mendoza L, Reséndiz M, Pinelli-Saavedra A, Mata-Haro V, Mwangi W, Hernández J. 2009. Induction of T helper 3 regulatory cells by dendritic cells infected with porcine reproductive and respiratory syndrome virus. Virology 387:373–379. https://doi.org/10.1016/j.virol.2009.02.033.
73. Dinarello CA, Novick D, Kim S, Kaplanski G. 2013. Interleukin-18 and IL-18 binding protein. Front Immunol 4:289. https://doi.org/10.3389/fimmu.2013.00289.
74. Novick D, Kim SH, Fantuzzi G, Reznikov LL, Dinarello CA, Rubinstein M. 1999. Interleukin-18 binding protein: a novel modulator of the Th1 cytokine response. Immunity 10:127–136. https://doi.org/10.1016/s1074-7613(00)80013-8.
75. Rahe MC, Murtaugh MP. 2017. Mechanisms of adaptive immunity to porcine reproductive and respiratory syndrome virus. Viruses 9:148. https://doi.org/10.3390/v9060148.
76. Yue F, Cheng A, Zhu Y, Li P, Zhang Y, Sun G, Wang M, Wang X. 2015. Overexpression of programmed death ligands in naturally occurring post-weaning multisystemic wasting syndrome. Viral Immunol 28:101–106. https://doi.org/10.1089/vim.2014.0097.
77. Wykes MN, Lewin SR. 2018. Immune checkpoint blockade in infectious diseases. Nat Rev Immunol 18:91–104. https://doi.org/10.1038/nri.2017.112.
78. Henning AN, Roychoudhuri R, Restifo NP. 2018. Epigenetic control of CD8+ T cell differentiation. Nat Rev Immunol 18:340–356. https://doi.org/10.1038/nri.2017.146.
79. Kahan SM, Wherry EJ, Zajac AJ. 2015. T cell exhaustion during persistent viral infections. Virology 479–480:180–193. https://doi.org/10.1016/j.virol.2014.12.033.
80. Ruedas-Torres I, Rodríguez-Gómez IM, Sánchez-Carvajal JM, Guil-Luna S, Larenas-Muñoz F, Pallarés FJ, Carrasco L, Gómez-Laguna J. 2021. Up-regulation of immune checkpoints in the thymus of PRRSV-1-infected piglets in a virulence-dependent fashion. Front Immunol 12:1543.

81. Rodríguez-Gómez IM, Talker SC, Käser T, Stadler M, Hammer SE, Saalmüller A, Gerner W. 2016. Expression of T-bet, Eomesodermin and GATA-3 in porcine $\alpha\beta$ T cells. Dev Comp Immunol 60:115–126. https://doi.org/10.1016/j.dci.2016.02.022.
82. Li J, He Y, Hao J, Ni L, Dong C. 2018. High levels of eomes promote exhaustion of anti-tumor CD8+ T cells. Front Immunol 9:2981. https://doi.org/10.3389/fimmu.2018.02981.
83. Paley MA, Kroy DC, Odorizzi PM, Johnnidis JB, Dolfi DV, Barnett BE, Bikoff EK, Robertson EJ, Lauer GM, Reiner SL, Wherry EJ. 2012. Progenitor and terminal subsets of CD8+ T cells cooperate to contain chronic viral infection. Science 338:1220–1225. https://doi.org/10.1126/science.1229620.
84. Zhang J, Timoney PJ, MacLachlan NJ, McCollum WH, Balasuriya UBR. 2008. Persistent equine arteritis virus infection in HeLa cells. J Virol 82:8456–8464. https://doi.org/10.1128/JVI.01249-08.
85. Langfelder P, Mischel PS, Horvath S. 2013. When is hub gene selection better than standard meta-analysis? PLoS One 8:e61505. https://doi.org/10.1371/journal.pone.0061505.
86. Nandi D, Pathak S, Verma T, Singh M, Chattopadhyay A, Thakur S, Raghavan A, Gokhroo A, Vijayamahantesh. 2020. T cell costimulation, checkpoint inhibitors and anti-tumor therapy. J Biosci 45:50. https://doi.org/10.1007/s12038-020-0020-2.
87. Schönrich G, Raftery MJ. 2019. The PD-1/PD-L1 axis and virus infections: A delicate balance. Front Cell Infect Microbiol 9:207. https://doi.org/10.3389/fcimb.2019.00207.
88. Ward-Kavanagh LK, Lin WW, Šedý JR, Ware CF. 2016. The TNF receptor superfamily in co-stimulating and co-inhibitory responses. Immunity Cell Press 44:1005–1019. https://doi.org/10.1016/j.immuni.2016.04.019.
89. Schäfer A, Hühr J, Schwaiger T, Dorhoi A, Mettenleiter TC, Blome S, Schröder C, Blohm U. 2019. Porcine invariant natural killer T cells: Functional profiling and dynamics in steady state and viral infections. Front Immunol 10:1380. https://doi.org/10.3389/fimmu.2019.01380.
90. Wikenheiser DJ, Stumhofer JS. 2016. ICOS co-stimulation: friend or foe? Front Immunol 7:304. https://doi.org/10.3389/fimmu.2016.00304.
91. Gimeno M, Darwich L, Diaz I, De La Torre E, Pujols J, Martín M, Inumaru S, Cano E, Domingo M, Montoya M, Mateu E. 2011. Cytokine profiles and phenotype regulation of antigen presenting cells by genotype-I porcine reproductive and respiratory syndrome virus isolates. Vet Res 42:9. https://doi.org/10.1186/1297-9716-42-9.
92. Sibila M, Calsamiglia M, Segalés J, Blanchard P, Badiella L, Le Dimna M, Jestin A, Domingo M. 2004. Use of a polymerase chain reaction assay and an ELISA to monitor porcine circovirus type 2 infection in pigs from farms with and without postweaning multisystemic wasting syndrome. Am J Vet Res 65:88–92. https://doi.org/10.2460/ajvr.2004.65.88.
93. Mattsson JG, Bergstrom K, Wallgren P, Johansson K-EE, Bergström K, Wallgren P, Johansson K-E. 1995. Detection of Mycoplasma hyopneumoniae in nose swabs from pigs by in vitro amplification of the 16S rRNA gene. J Clin Microbiol 33:893–897. https://doi.org/10.1128/jcm.33.4.893-897.1995.
94. Halbur PG, Paul PS, Meng X-J, Lum MA, Andrews JJ, Rathje JA. 1996. Comparative pathogenicity of nine US porcine reproductive and respiratory syndrome virus (PRRSV) isolates in a five-week-old cesarean-derived, colostrum-deprived pig model. J Vet Diagn Invest 8:11–20. https://doi.org/10.1177/104063879600800103.
95. Kuzemtseva L, de la Torre E, Martín G, Soldevila F, Ait-Ali T, Mateu E, Darwich L. 2014. Regulation of toll-like receptors 3, 7 and 9 in porcine alveolar macrophages by different genotype 1 strains of porcine reproductive and respiratory syndrome virus. Vet Immunol Immunopathol 158:189–198. https://doi.org/10.1016/j.vetimm.2014.01.009.
96. Falgueras J, Lara AJ, Fernández-Pozo N, Cantón FR, Pérez-Trabado G, Claros MG. 2010. SeqTrim: a high-throughput pipeline for pre-processing any type of sequence read. BMC Bioinformatics 11:38. https://doi.org/10.1186/1471-2105-11-38.
97. Nueda MJ, Martorell-Marugan J, Martí C, Tarazona S, Conesa A. 2018. Identification and visualization of differential isoform expression in RNA-seq time series. Bioinformatics 34:524–526. https://doi.org/10.1093/bioinformatics/btx578.
98. González Gayte I, Bautista Moreno R, Seoane Zonjic P, Claros MG. 2017. DEgenes Hunter—A flexible R pipeline for automated RNA-seq studies in organisms without reference genome. Genomics Comput Biol 3:31. https://doi.org/10.18547/gcb.2017.vol3.iss3.e31.
99. Mlecnik B, Galon J, Bindea G. 2018. Comprehensive functional analysis of large lists of genes and proteins. J Proteomics 171:2–10. https://doi.org/10.1016/j.jprot.2017.03.016.
100. Bindea G, Mlecnik B, Hackl H, Charoentong P, Tosolini M, Kirilovsky A, Fridman W-H, Pagès F, Trajanoski Z, Galon J. 2009. ClueGO: a Cytoscape plug-in to decipher functionally grouped gene ontology and pathway annotation networks. Bioinformatics 25:1091–1093. https://doi.org/10.1093/bioinformatics/btp101.
101. Szklarczyk D, Gable AL, Lyon D, Junge A, Wyder S, Huerta-Cepas J, Simonovic M, Doncheva NT, Morris JH, Bork P, Jensen LJ, Von Mering C. 2019. STRING v11: protein–protein association networks with increased coverage, supporting functional discovery in genome-wide experimental datasets. Nucleic Acids Res 47:D607–D613. https://doi.org/10.1093/nar/gky1131.
102. Shannon P, Markiel A, Ozier O, Baliga NS, Wang JT, Ramage D, Amin N, Schwikowski B, Ideker T. 2003. Cytoscape: a software Environment for integrated models of biomolecular interaction networks. Genome Res 13:2498–2504. https://doi.org/10.1101/gr.1239303.
103. Chin CH, Chen SH, Wu HH, Ho CW, Ko MT, Lin CY. 2014. *cytoHubba*: identifying hub objects and sub-networks from complex interactome. BMC Syst Biol 8:S11. https://doi.org/10.1186/1752-0509-8-S4-S11.
104. Schmittgen TD, Livak KJ. 2008. Analyzing real-time PCR data by the comparative CT method. Nat Protoc 3:1101–1108. https://doi.org/10.1038/nprot.2008.73.
105. Duvigneau JC, Hartl RT, Groiss S, Gemeiner M. 2005. Quantitative simultaneous multiplex real-time PCR for the detection of porcine cytokines. J Immunol Methods 306(1-2):16–27. https://doi.org/10.1016/j.jim.2005.06.021.
106. Yue F, Zhu YP, Zhang YF, Sun GP, Yang Y, Guo DG, et al. 2014. Up-regulated expression of PD-1 and its ligands during acute classical swine fever virus infection in swine. Res Vet Sci 97:251–256. https://doi.org/10.1016/j.rvsc.2014.07.023.
107. Royaee AR, Husmann RJ, Dawson HD, Calzada-Nova G, Schnitzlein WM, Zuckermann FA, Lunney JK. 2004. Deciphering the involvement of innate immune factors in the development of the host response to PRRSV vaccination. Vet Immunol Immunopathol 102:199–216. https://doi.org/10.1016/j.vetimm.2004.09.018.
108. Bordet E, Blanc F, Tiret M, Crisci E, Bouguyon E, Renson P, et al. 2018. Porcine reproductive and respiratory syndrome virus type 1.3 Lena triggers conventional dendritic cells 1 activation and T helper 1 immune response without infecting dendritic cells. Front Immunol 9:2299. https://doi.org/10.3389/fimmu.2018.02299.